

CERN-EP-2024-187
11 July 2024

Rapidity dependence of antideuteron coalescence in pp collisions at $\sqrt{s} = 13 \text{ TeV}$ with ALICE

ALICE Collaboration*

Abstract

The production yields of antideuterons and antiprotons are measured in pp collisions at a center-of-mass energy of $\sqrt{s} = 13 \text{ TeV}$, as a function of transverse momentum (p_T) and rapidity (y), for the first time rapidly-differentially up to $|y| = 0.7$. The measured spectra are used to study the p_T and rapidity dependence of the coalescence parameter B_2 , which quantifies the coalescence probability of antideuterons. The p_T and rapidity dependence of the obtained B_2 is extrapolated for $p_T > 1.7 \text{ GeV}/c$ and $|y| > 0.7$ using the phenomenological antideuteron production model implemented in PYTHIA 8.3 as well as a baryon coalescence afterburner model based on EPOS 3. Such measurements are of interest to the astrophysics community, since they can be used for the calculation of the flux of antinuclei from cosmic rays, in combination with coalescence models.

1 Introduction

Antinuclei such as antideuterons and antihelium still elude detection in space and, if discovered, would likely open the door to the indirect detection of weakly interacting dark-matter (DM) candidates [1, 2]. Other scenarios speculate about the existence of anticlouds or antistars as another possible explanation of antinuclei in space [3]. Indeed, the possible presence of antinuclei in our Galaxy could be explained either by reactions of high-energy cosmic rays (CRs) with the interstellar medium (ISM) or by more exotic sources such as decays/annihilations of DM candidates. Proton–proton (pp) and proton–nucleus (p–A) collisions are notably interesting in such a context, since the collisions between CRs and the ISM are the most relevant sources for the formation of nuclei in the Galaxy, because both, CRs and the ISM, consist mostly of hydrogen ($\sim 90\%$) and helium ($\sim 9\%$), and only in small percentage of heavier nuclei. The observation of a significant antimatter excess with respect to the expected background of antimatter produced in ordinary cosmic-ray interactions would represent a signal for dark-matter annihilation in the galactic halo or for the existence of antimatter islands in our Universe [3, 4].

Information on the production of antinuclei from accelerator experiments, particularly in small collision systems (i.e., pp and p–A collisions), is essential for the theoretical description of the background constituted by antinuclei from cosmic-ray collisions with ISM. Since the ISM is almost at rest and the CRs have kinetic energies peaked at around 300 GeV, the values of relevant center-of-mass energies per nucleon–nucleon collision for the antideuteron production range from $\sqrt{s_{\text{NN}}} \sim 17$ GeV to several TeV [5].

The goal of the existing experimental programs at different accelerator facilities is to obtain antinucleus production cross sections for pp and p–A reactions over a broad range of kinetic energies, to cover as much as possible the energy range spanned by the cosmic rays. To this end, several experiments have measured the production of (anti)nuclei in different collision systems and center-of-mass energies. These include the low collision energies of the AGS [6–9], SPS [10], and RHIC [11–16], and the TeV scale energies of the Large Hadron Collider (LHC) [17–37]. Such measurements are crucial for correct interpretations of any future measurement in satellite and balloon-borne experiments, such as AMS-02 [38], GAPS [39], or BESS-Polar [40]. An ultimate goal of the experimental programs at accelerators is to pin down the microscopic production process of antinuclei in hadronic collisions or DM decay. In fact, the production mechanism of light (anti)nuclei in high-energy hadronic collisions is still not clear and much debated in the scientific community. The plethora of experimental data collected in the last decade is typically described using two different phenomenological models: the statistical hadronization model (SHM) and the baryon coalescence approach. In the SHM [41–47], light (anti)nuclei, as well as other hadron species, are assumed to be emitted by a source in local thermal and hydrochemical equilibrium with their abundances being fixed at the moment of the chemical freeze-out of the system created in the collision, at a temperature of $T_{\text{chem}} \sim 156$ MeV [48]. This model provides an excellent description of the measured hadron yields in central nucleus–nucleus collisions [45]. However, SHM struggles to reproduce the evolution with the charged-particle multiplicity of the ratios between integrated yields of nuclei and those of protons, especially for nuclei with masses $A \geq 3$ [34, 35, 49]. In the coalescence model [50–56], multi-baryon states are assumed to be formed by coalescence of baryons that are close in phase space at kinetic freeze-out, which occurs at a later time than the chemical freeze-out. In the simplest implementations of coalescence, only the momentum correlations are considered and the bound states are formed if the difference in momentum among the nucleons lies below a given threshold, namely the coalescence momentum p_0 . In the state-of-the-art implementations of the coalescence approach, the quantum-mechanical properties of the constituent baryons and of the final bound states are taken into account and the coalescence probability is calculated from the overlap between the wave functions of individual (point-like) baryons and the Wigner density of the final-state cluster [57].

From the experimental point of view, the coalescence probability is related to the coalescence parameter B_A , which is obtained from the ratio of the invariant yield of the nuclei with mass number A and that

of the protons raised to the power of A , assuming protons and neutrons to have the same transverse momentum distributions as they are isospin partners, and $p_T^p = p_T^A/A$

$$B_A = \left(\frac{1}{2\pi p_T^A} \left(\frac{d^2N}{dy dp_T} \right)_A \right) / \left(\frac{1}{2\pi p_T^p} \left(\frac{d^2N}{dy dp_T} \right)_p \right)^A. \quad (1)$$

The production of (anti)nuclei at the LHC was so far measured in the midrapidity region $|y| < 0.5$, and then, combined with several coalescence models, employed to predict the flux of antinuclei from CR interactions at forward rapidity. However, the possible impact of a rapidity dependence of the production yield and of the coalescence probability of antinuclei was suggested in Ref. [58]. Previous measurements of the production of (anti)protons and (anti)deuterons in different rapidity intervals have been carried out in heavy-ion collisions at RHIC energies by the BRAHMS Collaboration [13]. In this Letter we report the first measurements of the rapidity dependence of the production yield of \bar{p} and \bar{d} and of the coalescence parameter B_2 (obtained from Eq. 1 with $A = 2$) carried out in pp collisions at LHC energies.

The results presented in this Letter contribute to the understanding of the impact that the extrapolation of the production yield and coalescence probability at forward rapidity, constrained to experimental information, has on the flux of antinuclei from cosmic rays, which can be obtained using hadronic production mechanisms based on coalescence. By measuring the production of antideuterons and antiprotons as a function of rapidity in pp collisions at $\sqrt{s} = 13$ TeV up to $|y| = 0.7$, the extrapolation at forward rapidity and high p_T/A of the coalescence parameter B_2 is performed using several coalescence models. Given the sensitivity of the cosmic-ray experiments discussed above, i.e., AMS-02, GAPS, and BESS-Polar, and the current experimental uncertainties on the production measurements, the direct impact of these results on cosmological DM research is related to a better understanding of the antideuteron background flux [59], which needs to be precisely modeled to interpret future measurements of antideuteron CR flux correctly.

2 Experimental apparatus

ALICE is one of the four large experiments at the LHC and is dedicated to the study of hadronic collisions at ultra-relativistic energies. A detailed description of the ALICE apparatus and its performance can be found in Refs. [60, 61]. In the following, only the sub-detector systems used for this analysis are described.

Trajectories of charged particles are reconstructed in the ALICE central barrel, which covers the pseudo-rapidity interval of $|\eta| < 0.9$, with the Inner Tracking System (ITS) [60], the Time Projection Chamber (TPC) [62], and the Time-Of-Flight (TOF) detector [63]. These detectors are located inside a solenoidal magnet, which generates a highly homogeneous magnetic field of 0.5 T, parallel to the beam line.

The ITS consists of six cylindrical layers of silicon detectors and is used for the determination of primary and secondary vertices, and for charged-particle tracking. The TPC is a gas detector used for charged-particle track reconstruction and momentum determination, and particle identification via the measurement of the specific energy loss (dE/dx) of particles in the detector gas. The dE/dx resolution depends on the event multiplicity and is about 5%–6.5% for minimum-ionizing particles crossing the full volume of the TPC [61]. The particle identification is extended at high p_T using the TOF detector, which is located at a radial distance of 3.7 m from the nominal interaction point. It measures the arrival time of particles relative to the event collision time provided by the TOF detector itself or by the T0 detectors. The T0 consists of two arrays of Cherenkov counters, T0A and T0C, located on opposite sides of the interaction point, covering the pseudorapidity regions $4.6 < \eta < 4.9$ and $-3.3 < \eta < -3.0$. A weighted average is performed when both T0 and TOF detectors have measured the start time [64]. The TOF time resolution is 56 ps [63].

Collision events are triggered by two plastic scintillator arrays, V0A and V0C [65], located at asymmetric positions, one on each side of the interaction point, covering the pseudorapidity regions $-3.7 < \eta < -1.7$ and $2.8 < \eta < 5.1$. Each V0 array consists of four rings in the radial direction, with each ring comprising eight cells with the same azimuthal size. The V0 detector is used to define the minimum-bias (MB) trigger (requiring coincident signals in the V0 detectors to be synchronous with the bunch-crossing time defined by the LHC clock). The V0 is also used to reject background events like beam–gas interactions, collisions with de-bunched protons, or with mechanical structures of the beam line [65].

3 Data analysis

The analyzed data sample was collected in 2016, 2017, and 2018 during the LHC pp run at $\sqrt{s} = 13$ TeV. Events with multiple vertices identified from track segments in the two innermost layers of the ITS are tagged as pile-up and removed from the analysis [61]. In order to ensure full geometrical acceptance in the ITS for $|\eta| < 0.9$ and reject background collisions, the coordinate of the primary vertex along the beam axis is required to be within 10 cm from the nominal interaction point. A total number of approximately 1.7 billion MB pp events were analyzed, with a total integrated luminosity of about 22 nb^{-1} [66].

The reconstructed tracks are required to fulfill the same set of quality criteria of the corresponding analyses of antiprotons and antideuteron production at midrapidity [28, 67], with the only difference that in the case of the present analysis no selections in pseudorapidity are applied, besides the ones enforced by the detector acceptance ($|\eta| < 0.9$ in the ALICE central barrel). The antiproton (antideuteron) identification is done at $p_T < 0.7 \text{ GeV}/c$ ($p_T < 1.2 \text{ GeV}/c$) by requiring that its energy loss per unit of track length measured by the TPC is within $3\sigma_{dE/dx}$ from the expected average for antiprotons (antideuterons), where $\sigma_{dE/dx}$ is the dE/dx resolution. For $p_T > 0.7 \text{ GeV}/c$ for antiprotons and $p_T > 1.2 \text{ GeV}/c$ for antideuterons, the dE/dx signal of the TPC is complemented by the time-of-flight measured by the TOF detector. The antiproton (antideuteron) signal is extracted from a fit to the $n(\sigma^{\text{TOF}}) = (t^{\text{TOF}} - t_{\exp}^{\text{TOF}})/\sigma_t$ distribution, where t^{TOF} is the measured time-of-flight, t_{\exp}^{TOF} its expected value for protons (deuterons), divided by the resolution on the time-of-flight measurement (σ_t). The fit function consists of a Gaussian with an exponential tail for the signal and the sum of two exponential functions for the background. The raw signal yield is extracted by integrating the signal function in the asymmetric interval $[-3\sigma^{\text{TOF}} + \mu_0, 3.5\sigma^{\text{TOF}} + \mu_0]$, where μ_0 is the mean of the Gaussian. The acceptance of the ITS, TPC, and TOF detectors ($|\eta| < 0.9$) limits the rapidity coverage of the measurement. Hence, the analysis is performed in seven rapidity intervals, 0.2 units wide, from -0.7 to 0.7 . At $|y|$ larger than 0.7 , the acceptance of the TPC and TOF detectors allows for the reconstruction of deuterons only at high p_T (for $|y| = 0.8$, the minimum p_T of deuterons that can be reconstructed is $\sim 3.5 \text{ GeV}/c$). However, in the high p_T region ($p_T > 3.5 \text{ GeV}/c$) deuterons cannot be identified any longer because the background due to mismatched tracks in the TOF is dominant with respect to the actual signal. The amount of observed raw antiprotons is about 2×10^5 in each of the first five rapidity classes ($|y| < 0.1$ to $0.4 < |y| < 0.5$), and decreasing to 1.5×10^5 and 1×10^5 in the two highest rapidity classes ($0.5 < |y| < 0.6$ and $0.6 < |y| < 0.7$, respectively). For antideuterons, the amount of observed raw counts is about 4×10^4 in each of the first four rapidity classes ($|y| < 0.1$ to $0.3 < |y| < 0.4$), and decreasing to 2×10^4 , 1×10^4 and 5×10^3 in the higher rapidity classes ($0.4 < |y| < 0.5$, $0.5 < |y| < 0.6$ and $0.6 < |y| < 0.7$, respectively). In both cases, the lower amount of observed antinuclei at high rapidity is due to the smaller transverse momentum coverage and lower acceptance and reconstruction efficiency.

The raw antiproton and antideuteron p_T spectra are corrected for the acceptance and reconstruction efficiency and, only for antiprotons, for the fraction of secondary antiprotons produced by feed-down of weak decays of $\bar{\Lambda}$ hyperons. Both corrections are calculated with Monte Carlo (MC) simulations in which antinuclei are embedded into pp collision events generated using PYTHIA 8.1 with the Monash 2013 tune [68]. Antinuclei are generated with uniform p_T and rapidity distributions in $(0 < p_T < 10) \text{ GeV}/c$

and $-1 < y < 1$. The particle interactions in the experimental apparatus are simulated using GEANT 4 as transport package [69]. The acceptance \times efficiency, in each p_T and rapidity interval, is calculated as the ratio of reconstructed and generated antiprotons and antinuclei in the simulation, where the same track selection and PID criteria as those used in the data are applied to the reconstructed sample in MC. The resulting acceptance \times efficiency depends on p_T , rapidity, and PID technique (either TPC only at low p_T , or TPC and TOF for $p_T > 0.7$ GeV/c for antiprotons, and for $p_T > 1.2$ GeV/c for antideuterons). For the class $|y| < 0.1$, it varies from $\sim 50\%$ at low p_T to about 25% at high p_T , for antiprotons, and from $\sim 80\%$ at low p_T to about 40% at high p_T , for antideuterons. For the class $0.6 < |y| < 0.7$, instead, the PID is done only with the TOF, and the acceptance \times efficiency varies from $\sim 10\%$ at low p_T to about 30% at high p_T , for antiprotons, and from $\sim 20\%$ at low p_T to about 45% at high p_T , for antideuterons.

In order to limit the contamination from secondary antiprotons from feed-down of weak decays, the measured distance of closest approach to the primary vertex in the transverse plane (DCA_{xy}) and along the beam direction (DCA_z) is requested to be less than 0.1 cm and 1 cm, respectively. To remove any remaining contamination of antiprotons from weak decays, the secondary fraction is estimated in each p_T and rapidity interval by fitting the distributions of the DCA_{xy} , using the template method [18]. The DCA_{xy} template distributions of primary (produced in the collision at the primary vertex) and secondary antiprotons from feed-down are taken from MC simulations. The resulting primary fraction of antiprotons has a mild p_T dependence, ranging from $\sim 80\%$ at low p_T to $\sim 90\%$ at high p_T .

The sources of systematic uncertainties on the transverse momentum distributions considered for this analysis are related to (i) track selection and particle identification, (ii) detector material budget, (iii) TPC–ITS and TPC–TOF track matching efficiencies, (iv) hadronic interaction of antiparticles with the detector material, and (v) signal loss (to account for antiparticles lost in rejected events). The uncertainties related to (i) are estimated for the present analysis and discussed below, while the other ones are inherited, as relative uncertainties, from previous similar analyses. The uncertainties due to (ii) and (v) are estimated as described in Ref. [28], and those due to (iii) and (iv) are assessed as illustrated in Ref. [31].

In order to assess the systematic uncertainties related to the track selection, the analysis is repeated using 50 settings with different criteria. These criteria are defined by randomly sampling the analysis parameters from uniform probability distributions, such that their variations produce a raw yield variation of a maximum factor of two, in order to uniformly explore the full available phase-space. The efficiency-corrected yields are distributed according to a Gaussian and the standard deviation of this distribution is taken as systematic uncertainty. The uncertainties connected to the particle identification are given by two contributions. One is estimated by extending or narrowing the integration intervals by $\pm 1\sigma$ and it is determined by calculating the standard deviation of the distribution of the fully corrected yields, in each p_T and rapidity interval, similarly to what was done in Ref. [28]. In addition, it is included the small contribution ($\sim 1\%$) due to the difference between the yield extracted by the integral of the fit function which describes the signal and that of the histogram after the subtraction of the background. In the case of antiprotons, also the contribution related to the secondary fraction of antiprotons from weak decays is included in (i), hence the uncertainty is larger for antiprotons than for antideuterons. For this uncertainty, the DCA selection criteria (both in the perpendicular plane DCA_{xy} , and along the beam axis DCA_z) are also changed 50 times, and each time the corresponding primary fraction is used for correction. The total systematic uncertainties are obtained by summing in quadrature all the individual contributions, which are summarized in Table 1. Within the studied rapidity range, the systematic uncertainties have been found to be independent of the analyzed rapidity interval.

Table 1: Summary of the systematic uncertainties on the transverse momentum distributions. The values reported in the table correspond to the uncertainties of the rapidity class $|y| < 0.1$. For such class, low p_T corresponds to 0.375 GeV/c for antiprotons and to 0.75 GeV/c for antideuterons, whereas high p_T corresponds to 1.95 GeV/c for antiprotons and to 3.2 GeV/c for antideuterons.

| Source of uncertainty | \bar{p} low p_T | \bar{p} high p_T | \bar{d} low p_T | \bar{d} high p_T |
|-----------------------|---------------------|----------------------|---------------------|----------------------|
| Tracking and PID | 4.5% | 6% | 1.5% | 3% |
| Material budget | <1% | <1% | <1% | <1% |
| Matching efficiencies | 3% | 3% | 1% | 2.5% |
| Hadronic interaction | 2% | 2% | 3% | 4% |
| Signal loss | – | – | 1% | <1% |
| Total | 6% | 7% | 4% | 6% |

4 Results

The p_T -differential yields per unit of rapidity ($d^2N/dp_T dy$) of antiprotons and antideuterons in MB events and analyzed rapidity intervals are shown in Fig. 1. The results are consistent with those measured in $|y| < 0.5$ [28, 67]. The final transverse-momentum distributions are fitted using the Lévy–Tsallis function [70] to extrapolate the yields to the unmeasured regions. The Lévy–Tsallis fits of the spectra in the high-rapidity intervals ($|y| \geq 0.5$) are constrained to the spectrum in the lowest rapidity interval ($|y| < 0.1$), such that the normalization is always adjusted during the fit while the shape is constrained to the spectrum at low rapidity, which covers a broader p_T range. This procedure assumes that the shape of the p_T spectra is independent of rapidity, and this assumption was validated by the rather stable χ^2/NDF values of the fits across the studied rapidity interval. In order to obtain the integrated yields, the integrals of the data points of the transverse momentum spectra in the measured regions are summed to the integrals of the fit functions at low (down to 0) and high (up to 10 GeV/c) p_T . The resulting p_T -integrated yields (dN/dy) of antiprotons and antideuterons are shown in Fig. 2. The measured integrated yields of both species show a flat trend with rapidity, up to $|y| = 0.7$. The antiproton integrated yields as a function of rapidity are compared with the predictions of two event generators, namely PYTHIA 8 [68], with two different tunes (described in the following), and EPOS 3 [71, 72]. The measured antideuteron yields are compared with the predictions of three models, based on different assumptions and making use of different event generators. Two of these models use PYTHIA 8 [68] as event generator, the third EPOS 3 [71, 72]. While for antiprotons the event generators produce the desired particles directly, there are no antideuterons natively in the MC and their production is included as an afterburner with the coalescence model, on top of the events generated using the two event generators. All models shown in Fig. 2 are normalized to data, by dividing the yields obtained with the simulations by a factor corresponding to the ratio between the measured yield and the simulated one in the lowest rapidity interval ($|y| < 0.1$), since the natural abundances of particles are not well reproduced by the event generators.

In the first approach, already used in Ref. [36] and described in detail in the corresponding Supplemental Material [73], the phase space distributions of antinucleons are generated with PYTHIA 8 with the Monash 2013 tune [68], and their p_T spectra are re-weighted to match the measured antiproton p_T spectra. In this simple model, all spatial correlations are ignored and the antideuteron is formed if an antiproton and an antineutron have a momentum difference below a given coalescence momentum $\Delta p < p_0$ in the antideuteron rest frame. The best estimate of the coalescence momentum for this model is $p_0 = (285 \pm 1)$ MeV/c [36]. The second approach is a reaction-based model [74], where antideuterons are generated by ordinary nuclear reactions between antinucleons produced in the collision with parameterized energy-dependent cross sections tuned on available experimental data [75], as implemented in the

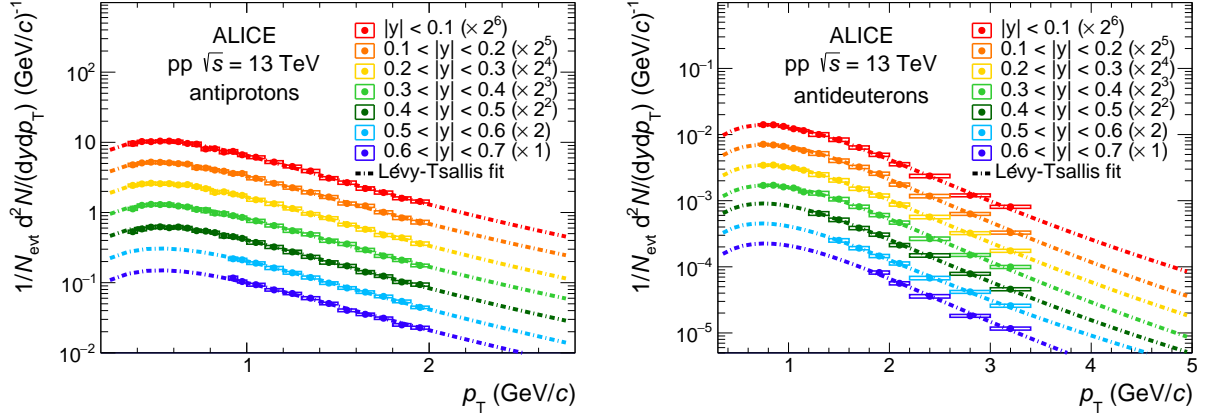


Figure 1: Antiproton (left panel) and antideuteron (right panel) p_T -differential yields for different rapidity intervals, in MB events. Statistical and systematic uncertainties are represented by vertical bars and boxes, respectively. The statistical uncertainties are smaller than the size of the markers in the reported scale and, hence, not visible. The dash-dotted lines represent the fit of the spectra executed with a Lévy–Tsallis function.

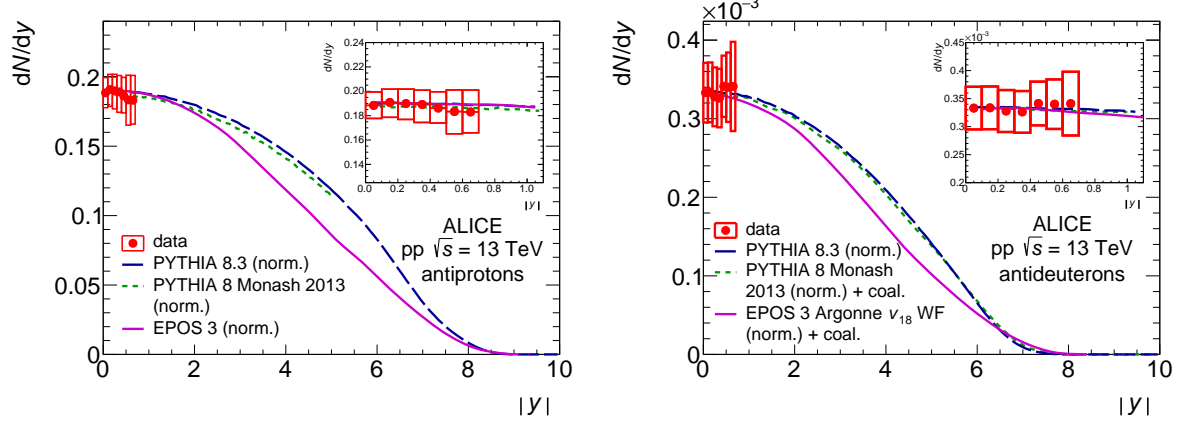


Figure 2: Integrated yields of antiprotons (left) and antideuterons (right) as a function of rapidity, compared with the corresponding predictions of three models (see text for details). Statistical and systematic uncertainties are represented by vertical bars and boxes, respectively. The statistical uncertainties are smaller than the size of the markers in the reported scale and, hence, not visible. In the insets of the figures, a zoom in the low-rapidity region is displayed. The integrated yields estimated by models are normalized to the measured ones, see text for details.

MC event generator PYTHIA 8.3. Both, the simple coalescence and the reaction-based model, are based on the simplistic assumption that coalescence can happen only if antiprotons and antineutrons are close in momentum space, while all spatial correlations are neglected, and the nucleus wave function does not come into play. The third approach is a state-of-the-art coalescence model [57] based on the Wigner function formalism, applied as an afterburner to the nucleons generated with the EPOS 3 event generator. In such a model, the quantum-mechanical properties of the nucleus are taken into account through its Wigner function. Antideuterons are formed following a probability calculated on an event-by-event basis, by folding the spatial distribution of nucleons with the Wigner function of the final bound state. The coalescence model is very sensitive to the source size, i.e., the size of the particle-emitting source that can be measured using femtoscopy with two-particle correlations [76]. Since the one implemented in EPOS 3 does not reproduce the measurements [57], a parameterization of the transverse-mass (m_T) dependence of the measured source size for high-multiplicity events ($r_0 = 1.249$ fm [77]) scaled to the minimum bias value ($r_0 = 1.18$ fm [78]) was used. It has to be noted that the average values of transverse mass, $\langle m_T \rangle$, of the high multiplicity sample (corresponding to the interval of 0–0.17% in multiplicity)

and of the minimum bias one (full multiplicity 0–100%) differ by $\sim 10\%$. Nonetheless, the source size is assumed to be independent of rapidity. Note also that the integrated yields predicted by the models are scaled to the data, while the shapes of the p_T distributions are not modified. Therefore, the models are no longer sensitive to the magnitude of the source size used for the calculations, but only to its m_T trend. Additionally, the predictions are obtained using the Argonne v_{18} wavefunction which was shown to give the best predictions for the antideuteron momentum distribution [57]. In this way, one obtains predictions using a realistic coalescence model, which considers not only the momentum distributions of nucleons but also their spatial correlations, as well as the quantum-mechanical nature of the coalescence process. The integrated yields of antiprotons and antideuterons as a function of rapidity obtained with the event generators and with the three models previously described show a similar trend, rather flat at low rapidities ($|y| < 1.5$) and decreasing starting from rapidity about 1.5, up to the kinematic limit of $|y| \sim 9.5$, related to the collision system and energy. However, while the predictions of the models based on PYTHIA 8 and simple coalescence are roughly equal in the full rapidity interval (0–9.5), a large difference, for rapidity larger than 1.5, is observed between these models and the third one in which the distributions of the antinucleons are obtained using EPOS 3 and a state-of-the-art model for deuteron formation via coalescence.

Using Eq. 1, the coalescence parameters B_2 in the different rapidity classes are calculated and shown in Fig. 3, in comparison with predictions from PYTHIA 8.3 (left panel) and from EPOS 3 with the coalescence model of Ref. [57] used as afterburner (right panel). For the computation of the uncertainties on the B_2 parameter, the invariant yields of antiprotons and antideuterons are considered uncorrelated and their uncertainties are propagated accordingly. The predictions obtained with PYTHIA 8 with the Monash 2013 tune have a negligible difference with respect to the predictions obtained with PYTHIA 8.3, and therefore not shown in the following. In the models, the antiproton p_T distributions are reweighted to the measured ones, while the antideuterons are only scaled to the integrated measured yields, and their p_T shapes are not changed. The rising trend of the coalescence parameters with p_T/A is well reproduced by the two models. Since larger coalescence parameters correspond to smaller source sizes (at higher p_T), this result reflects the observed decreasing trend of the source size with $\langle m_T \rangle$ [76].

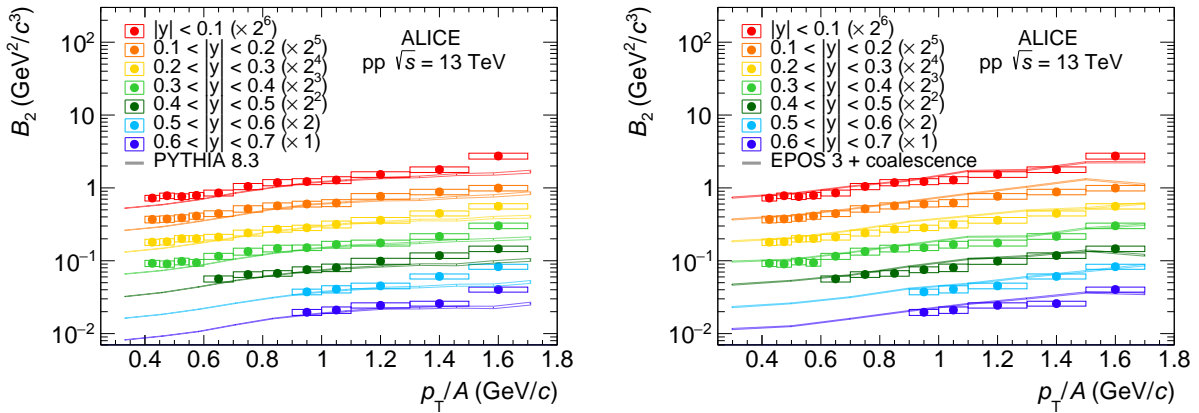


Figure 3: Coalescence parameter B_2 as a function of the transverse momentum per nucleon for different rapidity intervals. Data are compared to model predictions from PYTHIA 8.3 (left panel) and from a coalescence model [57] used as afterburner of EPOS 3 (right panel), shown as colored lines. Statistical and systematic uncertainties on the data points are represented by vertical bars and boxes, respectively. The statistical uncertainties of the data points are smaller than the size of the markers in the reported scale and, hence, not visible.

Finally, selecting intervals of p_T/A , it is interesting to look at the trend of the coalescence parameter as a function of rapidity. The rapidity dependence of B_2 is shown in Fig. 4 and compared with predictions from PYTHIA 8.3 (left panel) and from a coalescence model [57] used as afterburner of EPOS 3 (right panel). As for the yields, the coalescence parameter is flat in the rapidity region investigated by

the measurements. The models reproduce the measured trend, mostly with an agreement within 2σ . Some deviations beyond the 2σ level are present at high p_T/A (> 1.5 GeV/c) for the model based on PYTHIA 8.3. A similar trend of B_2 , flat as a function of rapidity, was also observed by the BRAHMS Collaboration in central Au–Au collisions at $\sqrt{s_{NN}} = 200$ GeV [13].

The models shown in Figs. 3 and 4 have similar statistical uncertainties, of about 10%, which are reflected in the width of the colored bands.

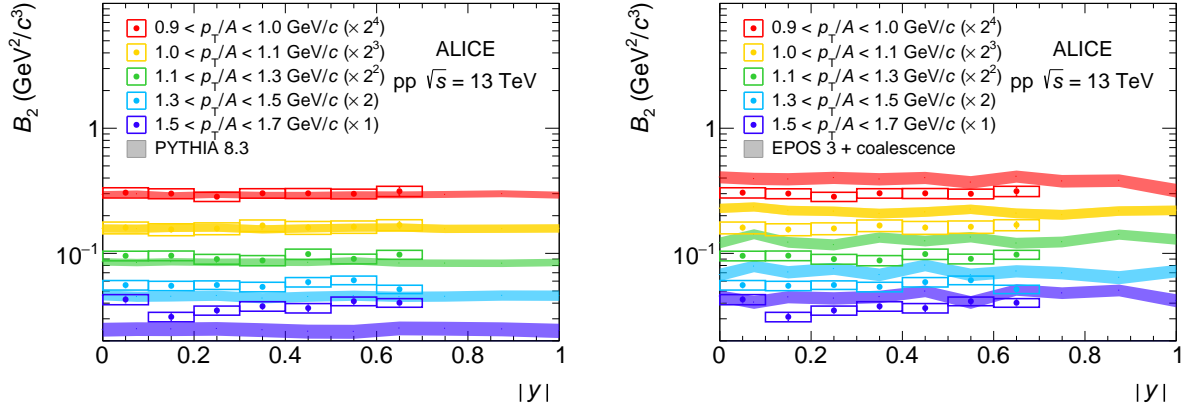


Figure 4: Coalescence parameter B_2 as a function of rapidity, for fixed transverse momentum per nucleon values. Statistical and systematic uncertainties on the data points are represented by vertical bars and boxes, respectively. The statistical uncertainties are smaller than the size of the markers in the reported scale and, hence, not visible. Bands show the model predictions from PYTHIA 8.3 (left panel) and from a coalescence model [57] used as afterburner of EPOS 3 (right panel), the width reflecting the statistical uncertainties.

The flux of antideuterons from cosmic rays as a function of rigidity, reported in Fig. 1 of Ref. [79], is predicted with the model of Ref. [4] using the coalescence parameter B_2 measured at midrapidity in pp collisions at $\sqrt{s} = 7$ TeV with ALICE [80]. The rapidity and p_T dependencies of the coalescence parameters predicted by PYTHIA 8.3 and EPOS 3, scaled to match the experimental measurements in the first p_T interval reported here, are extrapolated at high p_T ($p_T > 1.7$ GeV/c) and forward rapidity ($|y| > 0.7$) and provided to the authors of Refs. [4, 79]. In these models, the B_2 distributions are substantially flat as a function of rapidity and increase monotonically as a function of p_T/A . No difference is found in the shape of the antideuteron flux shown in Fig. 1 of Ref. [79], either using the different models presented in this Letter or using the B_2 measured at midrapidity in pp collisions at $\sqrt{s} = 7$ TeV [80]. A constant B_2 as a function of rapidity is a common assumption in several CR models. However, in the coalescence models presented in this work, the trend with rapidity of B_2 is investigated for the first time. Additionally, in Ref. [79], the author investigates the role of the rapidity extrapolation in predicting the cosmic ray flux of antinuclei (i.e., antiprotons, antideuterons, and antihelium-3), by setting the production cross section to zero in different kinematical regions. The results for the antideuteron flux from CR, presented in Fig. 1 of Ref. [79], show that at low kinetic energies, corresponding to rigidity $R \leq 5$ GV (being the rigidity defined as $R = \frac{pc}{Ze}$, where p is the momentum, c is the speed of light, and Ze is the charge of the cosmic-ray particle), about 90% of the flux is due to antideuterons with rapidity larger than 0.5. This kinematical region is also the one where the CR flux is expected to be dominated by the DM signal, according to many cosmological models [5], and hence of high impact for astrophysics. Therefore, it is important to measure the coalescence parameter in the rapidity region $|y| > 0.5$, in order to use experimental measurements as input for the astrophysical models. Moreover, the results of the antideuteron flux show that LHC experiments (such as LHCb [81–83] in its fixed-target configuration, and the future ALICE 3 facility [84]) are expected to fill the rapidity gap ($0.5 < |y| < 1.5$) providing measurements of production yields of antinuclei. These measurements would be of important use to the astrophysics community for the calculation of the flux of antinuclei from cosmic rays, to avoid relying

on the model extrapolation at forward rapidities.

5 Summary

In this Letter, the p_T -differential yields of antideuterons and antiprotons as a function of rapidity are measured in pp collisions at $\sqrt{s} = 13$ TeV, for the first time rapidly-differentially up to $|y| = 0.7$. Using the measured spectra, the p_T and rapidity dependence of the coalescence parameter B_2 is explored. Both the antiproton and antideuteron integrated yields, and the B_2 are found to be independent of rapidity in the measured range. The rapidity dependence of the obtained yields and B_2 is extrapolated for $|y| > 0.7$ using phenomenological antideuteron production models based on coalescence, making use of PYTHIA and EPOS 3 as event generators. The resulting predictions of B_2 as a function of p_T and rapidity are used as input for the model of Ref. [4], to investigate the role of the rapidity dependence of the coalescence parameter in the predictions of the flux of antinuclei from cosmic rays [79]. No impact on the predictions of the flux of antideuterons from CRs is seen when including the flat rapidity dependence of B_2 predicted with the models presented in this Letter, with respect to the predictions that use the B_2 measured at midrapidity in pp collisions at $\sqrt{s} = 7$ TeV [80]. However, as pointed out in Ref. [79], at low kinetic energies ($E_{\text{kin}} < 1$ GeV/nucleon) about 90% of the flux is due to antideuterons with rapidity between 0.5 and 1.5. Hence, the rapidity-dependent measurements of the production yields and coalescence probability of antinuclei in the region $0.5 < |y| < 1.5$ are a crucial input for CR models. These measurements have a fundamental impact on astrophysical indirect searches for dark matter, as the antinuclei produced from CR interactions are the dominant background source in the region of low kinetic energies. This measurement can be extended in the rapidity interval of interest by other facilities, present or future, such as LHCb [81, 83] and ALICE 3 [84].

Acknowledgements

The ALICE Collaboration would like to thank all its engineers and technicians for their invaluable contributions to the construction of the experiment and the CERN accelerator teams for the outstanding performance of the LHC complex. The ALICE Collaboration gratefully acknowledges the resources and support provided by all Grid centres and the Worldwide LHC Computing Grid (WLCG) collaboration. The ALICE Collaboration acknowledges the following funding agencies for their support in building and running the ALICE detector: A. I. Alikhanyan National Science Laboratory (Yerevan Physics Institute) Foundation (ANSL), State Committee of Science and World Federation of Scientists (WFS), Armenia; Austrian Academy of Sciences, Austrian Science Fund (FWF): [M 2467-N36] and Nationalstiftung für Forschung, Technologie und Entwicklung, Austria; Ministry of Communications and High Technologies, National Nuclear Research Center, Azerbaijan; Conselho Nacional de Desenvolvimento Científico e Tecnológico (CNPq), Financiadora de Estudos e Projetos (Finep), Fundação de Amparo à Pesquisa do Estado de São Paulo (FAPESP) and Universidade Federal do Rio Grande do Sul (UFRGS), Brazil; Bulgarian Ministry of Education and Science, within the National Roadmap for Research Infrastructures 2020-2027 (object CERN), Bulgaria; Ministry of Education of China (MOEC) , Ministry of Science & Technology of China (MSTC) and National Natural Science Foundation of China (NSFC), China; Ministry of Science and Education and Croatian Science Foundation, Croatia; Centro de Aplicaciones Tecnológicas y Desarrollo Nuclear (CEADEN), Cubaenergía, Cuba; Ministry of Education, Youth and Sports of the Czech Republic, Czech Republic; The Danish Council for Independent Research | Natural Sciences, the VILLUM FONDEN and Danish National Research Foundation (DNRF), Denmark; Helsinki Institute of Physics (HIP), Finland; Commissariat à l'Energie Atomique (CEA) and Institut National de Physique Nucléaire et de Physique des Particules (IN2P3) and Centre National de la Recherche Scientifique (CNRS), France; Bundesministerium für Bildung und Forschung (BMBF) and GSI Helmholtzzentrum für Schwerionenforschung GmbH, Germany; General Secretariat for Research and Technology, Ministry of Education, Research and Religions, Greece; National Research, Devel-

opment and Innovation Office, Hungary; Department of Atomic Energy Government of India (DAE), Department of Science and Technology, Government of India (DST), University Grants Commission, Government of India (UGC) and Council of Scientific and Industrial Research (CSIR), India; National Research and Innovation Agency - BRIN, Indonesia; Istituto Nazionale di Fisica Nucleare (INFN), Italy; Japanese Ministry of Education, Culture, Sports, Science and Technology (MEXT) and Japan Society for the Promotion of Science (JSPS) KAKENHI, Japan; Consejo Nacional de Ciencia (CONACYT) y Tecnología, through Fondo de Cooperación Internacional en Ciencia y Tecnología (FONCICYT) and Dirección General de Asuntos del Personal Académico (DGAPA), Mexico; Nederlandse Organisatie voor Wetenschappelijk Onderzoek (NWO), Netherlands; The Research Council of Norway, Norway; Pontificia Universidad Católica del Perú, Peru; Ministry of Science and Higher Education, National Science Centre and WUT ID-UB, Poland; Korea Institute of Science and Technology Information and National Research Foundation of Korea (NRF), Republic of Korea; Ministry of Education and Scientific Research, Institute of Atomic Physics, Ministry of Research and Innovation and Institute of Atomic Physics and Universitatea Națională de Știință și Tehnologie Politehnica București, Romania; Ministry of Education, Science, Research and Sport of the Slovak Republic, Slovakia; National Research Foundation of South Africa, South Africa; Swedish Research Council (VR) and Knut & Alice Wallenberg Foundation (KAW), Sweden; European Organization for Nuclear Research, Switzerland; Suranaree University of Technology (SUT), National Science and Technology Development Agency (NSTDA) and National Science, Research and Innovation Fund (NSRF via PMU-B B05F650021), Thailand; Turkish Energy, Nuclear and Mineral Research Agency (TENMAK), Turkey; National Academy of Sciences of Ukraine, Ukraine; Science and Technology Facilities Council (STFC), United Kingdom; National Science Foundation of the United States of America (NSF) and United States Department of Energy, Office of Nuclear Physics (DOE NP), United States of America. In addition, individual groups or members have received support from: Czech Science Foundation (grant no. 23-07499S), Czech Republic; European Research Council (grant no. 950692), European Union; ICSC - Centro Nazionale di Ricerca in High Performance Computing, Big Data and Quantum Computing, European Union - NextGenerationEU; Academy of Finland (Center of Excellence in Quark Matter) (grant nos. 346327, 346328), Finland.

References

- [1] F. Donato, N. Fornengo, and P. Salati, “Anti-deuterons as a signature of supersymmetric dark matter”, *Phys. Rev. D* **62** (2000) 043003, arXiv:hep-ph/9904481.
- [2] T. Aramaki *et al.*, “Review of the theoretical and experimental status of dark matter identification with cosmic-ray antideuterons”, *Phys. Rept.* **618** (2016) 1–37, arXiv:1505.07785 [hep-ph].
- [3] V. Poulin, P. Salati, I. Cholis, M. Kamionkowski, and J. Silk, “Where do the AMS-02 antihelium events come from?”, *Phys. Rev. D* **99** (2019) 023016, arXiv:1808.08961 [astro-ph.HE].
- [4] K. Blum, K. C. Y. Ng, R. Sato, and M. Takimoto, “Cosmic rays, antihelium, and an old navy spotlight”, *Phys. Rev. D* **96** (2017) 103021, arXiv:1704.05431 [astro-ph.HE].
- [5] L. Šerkšnytė *et al.*, “Reevaluation of the cosmic antideuteron flux from cosmic-ray interactions and from exotic sources”, *Phys. Rev. D* **105** (2022) 083021, arXiv:2201.00925 [astro-ph.HE].
- [6] **E878** Collaboration, M. J. Bennett *et al.*, “Light nuclei production in relativistic Au + nucleus collisions”, *Phys. Rev. C* **58** (1998) 1155–1164.
- [7] **E802** Collaboration, L. Ahle *et al.*, “Proton and deuteron production in Au + Au reactions at 11.6 A GeV/c”, *Phys. Rev. C* **60** (1999) 064901.
- [8] **E864** Collaboration, T. A. Armstrong *et al.*, “Measurements of light nuclei production in 11.5 A GeV/c Au + Pb heavy ion collisions”, *Phys. Rev. C* **61** (2000) 064908, arXiv:nucl-ex/0003009.

- [9] **E864** Collaboration, T. A. Armstrong *et al.*, “Anti-deuteron yield at the AGS and coalescence implications”, *Phys. Rev. Lett.* **85** (2000) 2685–2688, arXiv:nucl-ex/0005001.
- [10] **NA52 (NEWMASS)** Collaboration, G. Ambrosini *et al.*, “Baryon and anti-baryon production in lead-lead collisions at 158 A GeV/c”, *Phys. Lett. B* **417** (1998) 202–210.
- [11] **STAR** Collaboration, C. Adler *et al.*, “Anti-deuteron and anti- ${}^3\text{He}$ production in $\sqrt{s_{\text{NN}}} = 130$ GeV Au–Au collisions”, *Phys. Rev. Lett.* **87** (2001) 262301, arXiv:nucl-ex/0108022. [Erratum: *Phys. Rev. Lett.* **87**, 279902 (2001)].
- [12] **PHENIX** Collaboration, S. S. Adler *et al.*, “Deuteron and antideuteron production in Au + Au collisions at 200 GeV”, *Phys. Rev. Lett.* **94** (2005) 122302, arXiv:nucl-ex/0406004.
- [13] **BRAHMS** Collaboration, I. Arsene *et al.*, “Rapidity dependence of deuteron production in Au+Au collisions at $\sqrt{s_{\text{NN}}} = 200$ GeV”, *Phys. Rev. C* **83** (2011) 044906, arXiv:1005.5427 [nucl-ex].
- [14] **STAR** Collaboration, H. Agakishiev *et al.*, “Observation of the antimatter helium-4 nucleus”, *Nature* **473** (2011) 353, arXiv:1103.3312 [nucl-ex]. [Erratum: Nature 475 (2011) 412].
- [15] **STAR** Collaboration, L. Adamczyk *et al.*, “Measurement of elliptic flow of light nuclei at $\sqrt{s_{\text{NN}}} = 200, 62.4, 39, 27, 19.6, 11.5$, and 7.7 GeV at the BNL Relativistic Heavy Ion Collider”, *Phys. Rev. C* **94** (2016) 034908, arXiv:1601.07052 [nucl-ex].
- [16] **STAR** Collaboration, J. Adam *et al.*, “Beam energy dependence of (anti-)deuteron production in Au + Au collisions at the BNL Relativistic Heavy Ion Collider”, *Phys. Rev. C* **99** (2019) 064905, arXiv:1903.11778 [nucl-ex].
- [17] **ALICE** Collaboration, J. Adam *et al.*, “Precision measurement of the mass difference between light nuclei and anti-nuclei”, *Nature Phys.* **11** (2015) 811–814, arXiv:1508.03986 [nucl-ex].
- [18] **ALICE** Collaboration, J. Adam *et al.*, “Production of light nuclei and anti-nuclei in pp and Pb–Pb collisions at energies available at the CERN Large Hadron Collider”, *Phys. Rev. C* **93** (2016) 024917, arXiv:1506.08951 [nucl-ex].
- [19] **ALICE** Collaboration, S. Acharya *et al.*, “Measurement of deuteron spectra and elliptic flow in Pb–Pb collisions at $\sqrt{s_{\text{NN}}} = 2.76$ TeV at the LHC”, *Eur. Phys. J. C* **77** (2017) 658, arXiv:1707.07304 [nucl-ex].
- [20] **ALICE** Collaboration, S. Acharya *et al.*, “Elliptic and triangular flow of (anti)deuterons in Pb–Pb collisions at $\sqrt{s_{\text{NN}}} = 5.02$ TeV”, *Phys. Rev. C* **102** (2020) 055203, arXiv:2005.14639 [nucl-ex].
- [21] **ALICE** Collaboration, S. Acharya *et al.*, “Production of deuterons, tritons, ${}^3\text{He}$ nuclei and their antinuclei in pp collisions at $\sqrt{s} = 0.9, 2.76$ and 7 TeV”, *Phys. Rev. C* **97** (2018) 024615, arXiv:1709.08522 [nucl-ex].
- [22] **ALICE** Collaboration, S. Acharya *et al.*, “Production of ${}^4\text{He}$ and ${}^4\overline{\text{He}}$ in Pb–Pb collisions at $\sqrt{s_{\text{NN}}} = 2.76$ TeV at the LHC”, *Nucl. Phys. A* **971** (2018) 1–20, arXiv:1710.07531 [nucl-ex].
- [23] **LHCb** Collaboration, R. Aaij *et al.*, “Measurement of Antiproton Production in pHe Collisions at $\sqrt{s_{\text{NN}}} = 110$ GeV”, *Phys. Rev. Lett.* **121** (2018) 222001, arXiv:1808.06127 [hep-ex].
- [24] **ALICE** Collaboration, S. Acharya *et al.*, “Multiplicity dependence of (anti-)deuteron production in pp collisions at $\sqrt{s} = 7$ TeV”, *Phys. Lett. B* **794** (2019) 50–63, arXiv:1902.09290 [nucl-ex].

- [25] ALICE Collaboration, S. Acharya *et al.*, “Multiplicity dependence of light (anti-)nuclei production in p–Pb collisions at $\sqrt{s_{\text{NN}}} = 5.02$ TeV”, *Phys. Lett. B* **800** (2020) 135043, arXiv:1906.03136 [nucl-ex].
- [26] ALICE Collaboration, S. Acharya *et al.*, “Measurement of the (anti-) ^3He elliptic flow in Pb–Pb collisions at $\sqrt{s_{\text{NN}}} = 5.02$ TeV”, *Phys. Lett. B* **805** (2020) 135414, arXiv:1910.09718 [nucl-ex].
- [27] ALICE Collaboration, S. Acharya *et al.*, “Production of (anti-) ^3He and (anti-) ^3H in p–Pb collisions at $\sqrt{s_{\text{NN}}} = 5.02$ TeV”, *Phys. Rev. C* **101** (2020) 044906, arXiv:1910.14401 [nucl-ex].
- [28] ALICE Collaboration, S. Acharya *et al.*, “(Anti-)deuteron production in pp collisions at $\sqrt{s} = 13$ TeV”, *Eur. Phys. J. C* **80** (2020) 889, arXiv:2003.03184 [nucl-ex].
- [29] ALICE Collaboration, S. Acharya *et al.*, “Elliptic and triangular flow of (anti)deuterons in Pb–Pb collisions at $\sqrt{s_{\text{NN}}} = 5.02$ TeV”, *Phys. Rev. C* **102** (2020) 055203, arXiv:2005.14639 [nucl-ex].
- [30] ALICE Collaboration, S. Acharya *et al.*, “Jet-associated deuteron production in pp collisions at $\sqrt{s} = 13$ TeV”, *Phys. Lett. B* **819** (2021) 136440, arXiv:2011.05898 [nucl-ex].
- [31] ALICE Collaboration, S. Acharya *et al.*, “Production of light (anti)nuclei in pp collisions at $\sqrt{s} = 13$ TeV”, *JHEP* **01** (2022) 106, arXiv:2109.13026 [nucl-ex].
- [32] ALICE Collaboration, S. Acharya *et al.*, “Production of light (anti)nuclei in pp collisions at $\sqrt{s} = 5.02$ TeV”, *Eur. Phys. J. C* **82** (2022) 289, arXiv:2112.00610 [nucl-ex].
- [33] ALICE Collaboration, S. Acharya *et al.*, “Hypertriton Production in p–Pb Collisions at $\sqrt{s_{\text{NN}}} = 5.02$ TeV”, *Phys. Rev. Lett.* **128** (2022) 252003, arXiv:2107.10627 [nucl-ex].
- [34] ALICE Collaboration, S. Acharya *et al.*, “Light (anti)nuclei production in Pb–Pb collisions at $\sqrt{s_{\text{NN}}} = 5.02$ TeV”, *Phys. Rev. C* **107** (2023) 064904, arXiv:2211.14015 [nucl-ex].
- [35] ALICE Collaboration, S. Acharya *et al.*, “Measurement of the production of (anti)nuclei in p–Pb collisions at $\sqrt{s_{\text{NN}}} = 8.16$ TeV”, *Phys. Lett. B* **846** (2023) 137795, arXiv:2212.04777 [nucl-ex].
- [36] ALICE Collaboration, S. Acharya *et al.*, “Enhanced Deuteron Coalescence Probability in Jets”, *Phys. Rev. Lett.* **131** (2023) 042301, arXiv:2211.15204 [nucl-ex].
- [37] ALICE Collaboration, S. Acharya *et al.*, “Measurement of anti- ^3He nuclei absorption in matter and impact on their propagation in the Galaxy”, *Nature Phys.* **19** (2023) 61–71, arXiv:2202.01549 [nucl-ex].
- [38] A. Kounine, “The Alpha Magnetic Spectrometer on the International Space Station”, *Int. J. Mod. Phys. E* **21** (2012) 1230005.
- [39] C. J. Hailey, “An indirect search for dark matter using antideuterons: the GAPS experiment”, *New J. Phys.* **11** (2009) 105022.
- [40] K. Abe *et al.*, “Measurement of the cosmic-ray antiproton spectrum at solar minimum with a long-duration balloon flight over Antarctica”, *Phys. Rev. Lett.* **108** (2012) 051102, arXiv:1107.6000 [astro-ph.HE].

- [41] J. Cleymans, S. Kabana, I. Kraus, H. Oeschler, K. Redlich, and N. Sharma, “Antimatter production in proton-proton and heavy-ion collisions at ultrarelativistic energies”, *Phys. Rev.* **C84** (2011) 054916, arXiv:1105.3719 [hep-ph].
- [42] A. Andronic, P. Braun-Munzinger, J. Stachel, and H. Stöcker, “Production of light nuclei, hypernuclei and their antiparticles in relativistic nuclear collisions”, *Phys. Lett.* **B697** (2011) 203–207, arXiv:1010.2995 [nucl-th].
- [43] F. Becattini, E. Grossi, M. Bleicher, J. Steinheimer, and R. Stock, “Centrality dependence of hadronization and chemical freeze-out conditions in heavy ion collisions at $\sqrt{s_{NN}} = 2.76$ TeV”, *Phys. Rev.* **C90** (2014) 054907, arXiv:1405.0710 [nucl-th].
- [44] V. Vovchenko and H. Stöcker, “Examination of the sensitivity of the thermal fits to heavy-ion hadron yield data to the modeling of the eigenvolume interactions”, *Phys. Rev.* **C95** (2017) 044904, arXiv:1606.06218 [hep-ph].
- [45] A. Andronic, P. Braun-Munzinger, K. Redlich, and J. Stachel, “Decoding the phase structure of QCD via particle production at high energy”, *Nature* **561** (2018) 321–330, arXiv:1710.09425 [nucl-th].
- [46] N. Sharma, J. Cleymans, B. Hippolyte, and M. Paradza, “A Comparison of p-p, p-Pb, Pb-Pb Collisions in the Thermal Model: Multiplicity Dependence of Thermal Parameters”, *Phys. Rev.* **C99** (2019) 044914, arXiv:1811.00399 [hep-ph].
- [47] V. Vovchenko, B. Dönigus, and H. Stoecker, “Canonical statistical model analysis of p-p, p -Pb, and Pb–Pb collisions at energies available at the CERN Large Hadron Collider”, *Phys. Rev. C* **100** (2019) 054906, arXiv:1906.03145 [hep-ph].
- [48] A. Andronic, P. Braun-Munzinger, B. Friman, P. M. Lo, K. Redlich, and J. Stachel, “The thermal proton yield anomaly in Pb–Pb collisions at the LHC and its resolution”, *Phys. Lett. B* **792** (2019) 304–309, arXiv:1808.03102 [hep-ph].
- [49] ALICE Collaboration, S. Acharya *et al.*, “Measurement of the production and elliptic flow of (anti)nuclei in Xe–Xe collisions at $\sqrt{s_{NN}} = 5.44$ TeV”, *Phys. Rev. C* **110** (2024) 064901, arXiv:2405.19826 [nucl-ex].
- [50] S. T. Butler and C. A. Pearson, “Deuterons from High-Energy Proton Bombardment of Matter”, *Phys. Rev.* **129** (1963) 836–842.
- [51] J. I. Kapusta, “Mechanisms for deuteron production in relativistic nuclear collisions”, *Phys. Rev. C* **21** (1980) 1301–1310.
- [52] R. Scheibl and U. W. Heinz, “Coalescence and flow in ultrarelativistic heavy ion collisions”, *Phys. Rev.* **C59** (1999) 1585–1602, arXiv:nucl-th/9809092 [nucl-th].
- [53] W. Zhao, L. Zhu, H. Zheng, C. M. Ko, and H. Song, “Spectra and flow of light nuclei in relativistic heavy ion collisions at energies available at the BNL Relativistic Heavy Ion Collider and at the CERN Large Hadron Collider”, *Phys. Rev.* **C98** (2018) 054905, arXiv:1807.02813 [nucl-th].
- [54] K. Blum and M. Takimoto, “Nuclear coalescence from correlation functions”, *Phys. Rev. C* **99** (2019) 044913, arXiv:1901.07088 [nucl-th].
- [55] K.-J. Sun, C. M. Ko, and B. Dönigus, “Suppression of light nuclei production in collisions of small systems at the Large Hadron Collider”, *Phys. Lett.* **B792** (2019) 132–137, arXiv:1812.05175 [nucl-th].

- [56] M. Kachelrieß, S. Ostapchenko, and J. Tjemmland, “Alternative coalescence model for deuteron, tritium, helium-3 and their antinuclei”, *Eur. Phys. J. A* **56** (2020) 4, arXiv:1905.01192 [hep-ph].
- [57] M. Mahlein, L. Barioglio, F. Bellini, L. Fabbietti, C. Pinto, B. Singh, and S. Tripathy, “A realistic coalescence model for deuteron production”, *Eur. Phys. J. C* **83** (2023) 804, arXiv:2302.12696 [hep-ex].
- [58] Z. Citron *et al.*, “Report from Working Group 5: Future physics opportunities for high-density QCD at the LHC with heavy-ion and proton beams”, *CERN Yellow Rep. Monogr.* **7** (2019) 1159–1410, arXiv:1812.06772 [hep-ph].
- [59] D.-M. Gomez-Coral, A. Menchaca Rocha, V. Grabski, A. Datta, P. von Doetinchem, and A. Shukla, “Deuteron and Antideuteron Production Simulation in Cosmic-Ray Interactions”, *Phys. Rev. D* **98** (2018) 023012, arXiv:1806.09303 [astro-ph.HE].
- [60] ALICE Collaboration, K. Aamodt *et al.*, “The ALICE experiment at the CERN LHC”, *JINST* **3** (2008) S08002.
- [61] ALICE Collaboration, B. Abelev *et al.*, “Performance of the ALICE Experiment at the CERN LHC”, *Int. J. Mod. Phys. A* **29** (2014) 1430044, arXiv:1402.4476 [nucl-ex].
- [62] J. Alme *et al.*, “The ALICE TPC, a large 3-dimensional tracking device with fast readout for ultra-high multiplicity events”, *Nucl. Instrum. Meth. A* **622** (2010) 316–367, arXiv:1001.1950 [physics.ins-det].
- [63] ALICE Collaboration, A. Akindinov *et al.*, “Performance of the ALICE Time-Of-Flight detector at the LHC”, *Eur. Phys. J. Plus* **128** (2013) 44.
- [64] ALICE Collaboration, J. Adam *et al.*, “Determination of the event collision time with the ALICE detector at the LHC”, *Eur. Phys. J. Plus* **132** (2017) 99, arXiv:1610.03055 [physics.ins-det].
- [65] ALICE Collaboration, E. Abbas *et al.*, “Performance of the ALICE VZERO system”, *JINST* **8** (2013) P10016, arXiv:1306.3130 [nucl-ex].
- [66] ALICE Collaboration, “ALICE 2016-2017-2018 luminosity determination for pp collisions at $\sqrt{s} = 13$ TeV”, <https://cds.cern.ch/record/2776672>.
- [67] ALICE Collaboration, S. Acharya *et al.*, “Multiplicity dependence of π , K, and p production in pp collisions at $\sqrt{s} = 13$ TeV”, *Eur. Phys. J. C* **80** (2020) 693, arXiv:2003.02394 [nucl-ex].
- [68] P. Skands, S. Carrazza, and J. Rojo, “Tuning PYTHIA 8.1: the Monash 2013 Tune”, *Eur. Phys. J. C* **74** (2014) 3024, arXiv:1404.5630 [hep-ph].
- [69] GEANT4 Collaboration, S. Agostinelli *et al.*, “GEANT4—a simulation toolkit”, *Nucl. Instrum. Meth. A* **506** (2003) 250–303.
- [70] C. Tsallis, “Possible Generalization of Boltzmann-Gibbs Statistics”, *J. Statist. Phys.* **52** (1988) 479–487.
- [71] K. Werner, I. Karpenko, T. Pierog, M. Bleicher, and K. Mikhailov, “Event-by-Event Simulation of the Three-Dimensional Hydrodynamic Evolution from Flux Tube Initial Conditions in Ultrarelativistic Heavy Ion Collisions”, *Phys. Rev. C* **82** (2010) 044904, arXiv:1004.0805 [nucl-th].

- [72] K. Werner, B. Guiot, I. Karpenko, and T. Pierog, “Analysing radial flow features in p-Pb and p-p collisions at several TeV by studying identified particle production in EPOS3”, *Phys. Rev. C* **89** (2014) 064903, arXiv:1312.1233 [nucl-th].
- [73] See Supplemental Material at
<https://journals.aps.org/prl/supplemental/10.1103/PhysRevLett.131.042301> for details on PYTHIA models.
- [74] C. Bierlich *et al.*, “A comprehensive guide to the physics and usage of PYTHIA 8.3”, arXiv:2203.11601 [hep-ph].
- [75] L. A. Dal and A. R. Raklev, “Alternative formation model for antideuterons from dark matter”, *Phys. Rev. D* **91** (2015) 123536, arXiv:1504.07242 [hep-ph]. [Erratum: Phys.Rev.D 92, 069903 (2015), Erratum: Phys.Rev.D 92, 089901 (2015)].
- [76] **ALICE** Collaboration, S. Acharya *et al.*, “Search for a common baryon source in high-multiplicity pp collisions at the LHC”, *Phys. Lett. B* **811** (2020) 135849, arXiv:2004.08018 [nucl-ex].
- [77] **ALICE** Collaboration, S. Acharya *et al.*, “Investigation of the p- Σ 0 interaction via femtoscopy in pp collisions”, *Phys. Lett. B* **805** (2020) 135419, arXiv:1910.14407 [nucl-ex].
- [78] **ALICE** Collaboration, S. Acharya *et al.*, “Study of the Λ - Λ interaction with femtoscopy correlations in pp and p-Pb collisions at the LHC”, *Phys. Lett. B* **797** (2019) 134822, arXiv:1905.07209 [nucl-ex].
- [79] K. Blum, “Rapidity dependence of nuclear coalescence: impact on cosmic ray antinuclei”, *Phys. Rev. C* **109** (2024) L031904, arXiv:2306.13165 [astro-ph.HE].
- [80] **ALICE** Collaboration, S. Acharya *et al.*, “Multiplicity dependence of (anti-)deuteron production in pp collisions at $\sqrt{s} = 7$ TeV”, *Phys. Lett. B* **794** (2019) 50–63, arXiv:1902.09290 [nucl-ex].
- [81] **LHCb** Collaboration, A. A. Alves, Jr. *et al.*, “The LHCb Detector at the LHC”, *JINST* **3** (2008) S08005.
- [82] **LHCb** Collaboration, R. Aaij *et al.*, “LHCb Detector Performance”, *Int. J. Mod. Phys. A* **30** (2015) 1530022, arXiv:1412.6352 [hep-ex].
- [83] **LHCb** Collaboration, R. Aaij *et al.*, “Helium identification with LHCb”, *JINST* **19** (2024) P02010, arXiv:2310.05864 [hep-ex].
- [84] **ALICE** Collaboration, “Letter of intent for ALICE 3: A next-generation heavy-ion experiment at the LHC”, arXiv:2211.02491 [physics.ins-det].

A The ALICE Collaboration

- S. Acharya ¹²⁷, D. Adamová ⁸⁶, A. Agarwal¹³⁵, G. Aglieri Rinella ³², L. Aglietta ²⁴, M. Agnello ²⁹, N. Agrawal ²⁵, Z. Ahammed ¹³⁵, S. Ahmad ¹⁵, S.U. Ahn ⁷¹, I. Ahuja ³⁶, A. Akindinov ¹⁴¹, V. Akishina³⁸, M. Al-Turany ⁹⁷, D. Aleksandrov ¹⁴¹, B. Alessandro ⁵⁶, H.M. Alfanda ⁶, R. Alfaro Molina ⁶⁷, B. Ali ¹⁵, A. Alici ²⁵, N. Alizadehvandchali ¹¹⁶, A. Alkin ¹⁰⁴, J. Alme ²⁰, G. Alocco ^{24,52}, T. Alt ⁶⁴, A.R. Altamura ⁵⁰, I. Altsybeevev ⁹⁵, J.R. Alvarado ⁴⁴, C.O.R. Alvarez⁴⁴, M.N. Anaam ⁶, C. Andrei ⁴⁵, N. Andreou ¹¹⁵, A. Andronic ¹²⁶, E. Andronov ¹⁴¹, V. Anguelov ⁹⁴, F. Antinori ⁵⁴, P. Antonioli ⁵¹, N. Apadula ⁷⁴, L. Aphectche ¹⁰³, H. Appelshäuser ⁶⁴, C. Arata ⁷³, S. Arcelli ²⁵, R. Arnaldi ⁵⁶, J.G.M.C.A. Arneiro ¹¹⁰, I.C. Arsene ¹⁹, M. Arslanbekov ¹³⁸, A. Augustinus ³², R. Averbeck ⁹⁷, D. Averyanov ¹⁴¹, M.D. Azmi ¹⁵, H. Baba ¹²⁴, A. Badalà ⁵³, J. Bae ¹⁰⁴, Y.W. Baek ⁴⁰, X. Bai ¹²⁰, R. Bailhache ⁶⁴, Y. Bailung ⁴⁸, R. Bala ⁹¹, A. Balbino ²⁹, A. Baldissari ¹³⁰, B. Balis ², D. Banerjee ⁴, Z. Banoo ⁹¹, V. Barbasova³⁶, F. Barile ³¹, L. Barioglio ⁵⁶, M. Barlou ⁷⁸, B. Barman ⁴¹, G.G. Barnaföldi ⁴⁶, L.S. Barnby ¹¹⁵, E. Barreau ¹⁰³, V. Barret ¹²⁷, L. Barreto ¹¹⁰, C. Bartels ¹¹⁹, K. Barth ³², E. Bartsch ⁶⁴, N. Bastid ¹²⁷, S. Basu ⁷⁵, G. Batigne ¹⁰³, D. Battistini ⁹⁵, B. Batyunya ¹⁴², D. Bauri ⁴⁷, J.L. Bazo Alba ¹⁰¹, I.G. Bearden ⁸³, C. Beattie ¹³⁸, P. Becht ⁹⁷, D. Behera ⁴⁸, I. Belikov ¹²⁹, A.D.C. Bell Hechavarria ¹²⁶, F. Bellini ²⁵, R. Bellwied ¹¹⁶, S. Belokurova ¹⁴¹, L.G.E. Beltran ¹⁰⁹, Y.A.V. Beltran ⁴⁴, G. Bencedi ⁴⁶, A. Bensaoula¹¹⁶, S. Beole ²⁴, Y. Berdnikov ¹⁴¹, A. Berdnikova ⁹⁴, L. Bergmann ⁹⁴, M.G. Besoiu ⁶³, L. Betev ³², P.P. Bhaduri ¹³⁵, A. Bhasin ⁹¹, B. Bhattacharjee ⁴¹, L. Bianchi ²⁴, J. Bielčík ³⁴, J. Bielčíková ⁸⁶, A.P. Bigot ¹²⁹, A. Bilandzic ⁹⁵, G. Biro ⁴⁶, S. Biswas ⁴, N. Bize ¹⁰³, J.T. Blair ¹⁰⁸, D. Blau ¹⁴¹, M.B. Blidaru ⁹⁷, N. Bluhme³⁸, C. Blume ⁶⁴, G. Boca ^{21,55}, F. Bock ⁸⁷, T. Bodova ²⁰, J. Bok ¹⁶, L. Boldizsár ⁴⁶, M. Bombara ³⁶, P.M. Bond ³², G. Bonomi ^{134,55}, H. Borel ¹³⁰, A. Borissov ¹⁴¹, A.G. Borquez Carcamo ⁹⁴, E. Botta ²⁴, Y.E.M. Bouziani ⁶⁴, L. Bratrud ⁶⁴, P. Braun-Munzinger ⁹⁷, M. Bregant ¹¹⁰, M. Broz ³⁴, G.E. Bruno ^{96,31}, V.D. Buchakchiev ³⁵, M.D. Buckland ⁸⁵, D. Budnikov ¹⁴¹, H. Buesching ⁶⁴, S. Bufalino ²⁹, P. Buhler ¹⁰², N. Burmasov ¹⁴¹, Z. Buthelezi ^{68,123}, A. Bylinkin ²⁰, S.A. Bysiak¹⁰⁷, J.C. Cabanillas Noris ¹⁰⁹, M.F.T. Cabrera¹¹⁶, M. Cai ⁶, H. Caines ¹³⁸, A. Caliva ²⁸, E. Calvo Villar ¹⁰¹, J.M.M. Camacho ¹⁰⁹, P. Camerini ²³, F.D.M. Canedo ¹¹⁰, S.L. Cantway ¹³⁸, M. Carabas ¹¹³, A.A. Carballo ³², F. Carnesecchi ³², R. Caron ¹²⁸, L.A.D. Carvalho ¹¹⁰, J. Castillo Castellanos ¹³⁰, M. Castoldi ³², F. Catalano ³², S. Cattaruzzi ²³, C. Ceballos Sanchez ¹⁴², R. Cerri ²⁴, I. Chakaberia ⁷⁴, P. Chakraborty ¹³⁶, S. Chandra ¹³⁵, S. Chapelard ³², M. Chartier ¹¹⁹, S. Chattopadhyay¹³⁵, S. Chattopadhyay ¹³⁵, S. Chattopadhyay ⁹⁹, M. Chen ³⁹, T. Cheng ^{97,6}, C. Cheshkov ¹²⁸, V. Chibante Barroso ³², D.D. Chinellato ¹¹¹, E.S. Chizzali ^{II,95}, J. Cho ⁵⁸, S. Cho ⁵⁸, P. Chochula ³², Z.A. Chochulska¹³⁶, D. Choudhury ⁴¹, P. Christakoglou ⁸⁴, C.H. Christensen ⁸³, P. Christiansen ⁷⁵, T. Chujo ¹²⁵, M. Ciacco ²⁹, C. Cicalo ⁵², M.R. Ciupek ⁹⁷, G. Clai^{III,51}, F. Colamaria ⁵⁰, J.S. Colburn ¹⁰⁰, D. Colella ³¹, A. Colelli³¹, M. Colocci ²⁵, M. Concas ³², G. Conesa Balbastre ⁷³, Z. Conesa del Valle ¹³¹, G. Contin ²³, J.G. Contreras ³⁴, M.L. Coquet ¹⁰³, P. Cortese ^{133,56}, M.R. Cosentino ¹¹², F. Costa ³², S. Costanza ^{21,55}, C. Cot ¹³¹, P. Crochet ¹²⁷, R. Cruz-Torres ⁷⁴, M.M. Czarnynoga¹³⁶, A. Dainese ⁵⁴, G. Dange³⁸, M.C. Danisch ⁹⁴, A. Danu ⁶³, P. Das ⁸⁰, P. Das ⁴, S. Das ⁴, A.R. Dash ¹²⁶, S. Dash ⁴⁷, A. De Caro ²⁸, G. de Cataldo ⁵⁰, J. de Cuveland³⁸, A. De Falco ²², D. De Gruttola ²⁸, N. De Marco ⁵⁶, C. De Martin ²³, S. De Pasquale ²⁸, R. Deb ¹³⁴, R. Del Grande ⁹⁵, L. Dello Stritto ³², W. Deng ⁶, K.C. Devereaux¹⁸, P. Dhankher ¹⁸, D. Di Bari ³¹, A. Di Mauro ³², B. Diab ¹³⁰, R.A. Diaz ^{142,7}, T. Dietel ¹¹⁴, Y. Ding ⁶, J. Ditzel ⁶⁴, R. Divià ³², Ø. Djupsland²⁰, U. Dmitrieva ¹⁴¹, A. Dobrin ⁶³, B. Dönigus ⁶⁴, J.M. Dubinski ¹³⁶, A. Dubla ⁹⁷, P. Dupieux ¹²⁷, N. Dzalaiova¹³, T.M. Eder ¹²⁶, R.J. Ehlers ⁷⁴, F. Eisenhut ⁶⁴, R. Ejima ⁹², D. Elia ⁵⁰, B. Erazmus ¹⁰³, F. Ercolelli ²⁵, B. Espagnon ¹³¹, G. Eulisse ³², D. Evans ¹⁰⁰, S. Evdokimov ¹⁴¹, L. Fabbietti ⁹⁵, M. Faggion ²³, J. Faivre ⁷³, F. Fan ⁶, W. Fan ⁷⁴, A. Fantoni ⁴⁹, M. Fasel ⁸⁷, A. Feliciello ⁵⁶, G. Feofilov ¹⁴¹, A. Fernández Téllez ⁴⁴, L. Ferrandi ¹¹⁰, M.B. Ferrer ³², A. Ferrero ¹³⁰, C. Ferrero ^{IV,56}, A. Ferretti ²⁴, V.J.G. Feuillard ⁹⁴, V. Filova ³⁴, D. Finogeev ¹⁴¹, F.M. Fionda ⁵², E. Flatland³², F. Flor ^{138,116}, A.N. Flores ¹⁰⁸, S. Foertsch ⁶⁸, I. Fokin ⁹⁴, S. Fokin ¹⁴¹, U. Follo ^{IV,56}, E. Fragiocomo ⁵⁷, E. Frajna ⁴⁶, U. Fuchs ³², N. Funicello ²⁸, C. Furget ⁷³, A. Furs ¹⁴¹, T. Fusayasu ⁹⁸, J.J. Gaardhøje ⁸³, M. Gagliardi ²⁴, A.M. Gago ¹⁰¹, T. Gahlaout⁴⁷, C.D. Galvan ¹⁰⁹, D.R. Gangadharan ¹¹⁶, P. Ganoti ⁷⁸, C. Garabatos ⁹⁷, J.M. Garcia⁴⁴, T. García Chávez ⁴⁴, E. Garcia-Solis ⁹, C. Gargiulo ³², P. Gasik ⁹⁷, H.M. Gaur ³⁸, A. Gautam ¹¹⁸, M.B. Gay Ducati ⁶⁶, M. Germain ¹⁰³, R.A. Gernhaeuser⁹⁵, C. Ghosh¹³⁵, M. Giacalone ⁵¹, G. Gioachin ²⁹, S.K. Giri¹³⁵, P. Giubellino ^{97,56}, P. Giubilato ²⁷, A.M.C. Glaenzer ¹³⁰, P. Glässel ⁹⁴, E. Glimos ¹²², D.J.Q. Goh⁷⁶, V. Gonzalez ¹³⁷, P. Gordeev ¹⁴¹, M. Gorgon ², K. Goswami ⁴⁸, S. Gotovac³³, V. Grabski ⁶⁷, L.K. Graczykowski ¹³⁶, E. Grecka ⁸⁶, A. Grelli ⁵⁹,

- C. Grigoras ³², V. Grigoriev ¹⁴¹, S. Grigoryan ^{142,1}, F. Grossa ³², J.F. Grosse-Oetringhaus ³², R. Grossos ⁹⁷, D. Grund ³⁴, N.A. Grunwald ⁹⁴, G.G. Guardiano ¹¹¹, R. Guernane ⁷³, M. Guilbaud ¹⁰³, K. Gulbrandsen ⁸³, J.J.W.K. Gumprecht ¹⁰², T. Gündem ⁶⁴, T. Gunji ¹²⁴, W. Guo ⁶, A. Gupta ⁹¹, R. Gupta ⁹¹, R. Gupta ⁴⁸, K. Gwizdziel ¹³⁶, L. Gyulai ⁴⁶, C. Hadjidakis ¹³¹, F.U. Haider ⁹¹, S. Haidlova ³⁴, M. Haldar ⁴, H. Hamagaki ⁷⁶, Y. Han ¹³⁹, B.G. Hanley ¹³⁷, J. Hansen ⁷⁵, M.R. Haque ⁹⁷, J.W. Harris ¹³⁸, A. Harton ⁹, M.V. Hartung ⁶⁴, H. Hassan ¹¹⁷, D. Hatzifotiadou ⁵¹, P. Hauer ⁴², L.B. Havener ¹³⁸, E. Hellbär ³², H. Helstrup ³⁷, M. Hemmer ⁶⁴, T. Herman ³⁴, S.G. Hernandez ¹¹⁶, G. Herrera Corral ⁸, S. Herrmann ¹²⁸, K.F. Hetland ³⁷, B. Heybeck ⁶⁴, H. Hillemanns ³², B. Hippolyte ¹²⁹, I.P.M. Hobus ⁸⁴, F.W. Hoffmann ⁷⁰, B. Hofman ⁵⁹, G.H. Hong ¹³⁹, M. Horst ⁹⁵, A. Horzyk ², Y. Hou ⁶, P. Hristov ³², P. Huhn ⁶⁴, L.M. Huhta ¹¹⁷, T.J. Humanic ⁸⁸, A. Hutson ¹¹⁶, D. Hutter ³⁸, M.C. Hwang ¹⁸, R. Ilkaev ¹⁴¹, M. Inaba ¹²⁵, G.M. Innocenti ³², M. Ippolitov ¹⁴¹, A. Isakov ⁸⁴, T. Isidori ¹¹⁸, M.S. Islam ⁹⁹, S. Iurchenko ¹⁴¹, M. Ivanov ¹³, M. Ivanov ⁹⁷, V. Ivanov ¹⁴¹, K.E. Iversen ⁷⁵, M. Jablonski ², B. Jacak ^{18,74}, N. Jacazio ²⁵, P.M. Jacobs ⁷⁴, S. Jadlovska ¹⁰⁶, J. Jadlovsky ¹⁰⁶, S. Jaelani ⁸², C. Jahnke ¹¹⁰, M.J. Jakubowska ¹³⁶, M.A. Janik ¹³⁶, T. Janson ⁷⁰, S. Ji ¹⁶, S. Jia ¹⁰, T. Jiang ¹⁰, A.A.P. Jimenez ⁶⁵, F. Jonas ⁷⁴, D.M. Jones ¹¹⁹, J.M. Jowett ^{32,97}, J. Jung ⁶⁴, M. Jung ⁶⁴, A. Junique ³², A. Jusko ¹⁰⁰, J. Kaewjai ¹⁰⁵, P. Kalinak ⁶⁰, A. Kalweit ³², A. Karasu Uysal ⁷², D. Karatovic ⁸⁹, N. Karatzenis ¹⁰⁰, O. Karavichev ¹⁴¹, T. Karavicheva ¹⁴¹, E. Karpechev ¹⁴¹, M.J. Karwowska ^{32,136}, U. Kebschull ⁷⁰, R. Keidel ¹⁴⁰, M. Keil ³², B. Ketzer ⁴², J. Keul ⁶⁴, S.S. Khade ⁴⁸, A.M. Khan ¹²⁰, S. Khan ¹⁵, A. Khanzadeev ¹⁴¹, Y. Kharlov ¹⁴¹, A. Khatun ¹¹⁸, A. Khuntia ³⁴, Z. Khuranova ⁶⁴, B. Kileng ³⁷, B. Kim ¹⁰⁴, C. Kim ¹⁶, D.J. Kim ¹¹⁷, E.J. Kim ⁶⁹, J. Kim ¹³⁹, J. Kim ⁵⁸, J. Kim ^{32,69}, M. Kim ¹⁸, S. Kim ¹⁷, T. Kim ¹³⁹, K. Kimura ⁹², A. Kirkova ³⁵, S. Kirsch ⁶⁴, I. Kisel ³⁸, S. Kiselev ¹⁴¹, A. Kisiel ¹³⁶, J.P. Kitowski ², J.L. Klay ⁵, J. Klein ³², S. Klein ⁷⁴, C. Klein-Bösing ¹²⁶, M. Kleiner ⁶⁴, T. Klemenz ⁹⁵, A. Kluge ³², C. Kobdaj ¹⁰⁵, R. Kohara ¹²⁴, T. Kollegger ⁹⁷, A. Kondratyev ¹⁴², N. Kondratyeva ¹⁴¹, J. Konig ⁶⁴, S.A. Konigstorfer ⁹⁵, P.J. Konopka ³², G. Kornakov ¹³⁶, M. Korwieser ⁹⁵, S.D. Koryciak ², C. Koster ⁸⁴, A. Kotliarov ⁸⁶, N. Kovacic ⁸⁹, V. Kovalenko ¹⁴¹, M. Kowalski ¹⁰⁷, V. Kozhuharov ³⁵, G. Kozlov ³⁸, I. Králik ⁶⁰, A. Kravčáková ³⁶, L. Krcal ^{32,38}, M. Krivda ^{100,60}, F. Krizek ⁸⁶, K. Krizkova Gajdosova ³², C. Krug ⁶⁶, M. Krüger ⁶⁴, D.M. Krupova ³⁴, E. Kryshen ¹⁴¹, V. Kučera ⁵⁸, C. Kuhn ¹²⁹, P.G. Kuijer ⁸⁴, T. Kumaoka ¹²⁵, D. Kumar ¹³⁵, L. Kumar ⁹⁰, N. Kumar ⁹⁰, S. Kumar ⁵⁰, S. Kundu ³², P. Kurashvili ⁷⁹, A. Kurepin ¹⁴¹, A.B. Kurepin ¹⁴¹, A. Kuryakin ¹⁴¹, S. Kushpil ⁸⁶, V. Kuskov ¹⁴¹, M. Kutyla ¹³⁶, A. Kuznetsov ¹⁴², M.J. Kweon ⁵⁸, Y. Kwon ¹³⁹, S.L. La Pointe ³⁸, P. La Rocca ²⁶, A. Lakhathok ¹⁰⁵, M. Lamanna ³², A.R. Landou ⁷³, R. Langoy ¹²¹, P. Larionov ³², E. Laudi ³², L. Lautner ^{32,95}, R.A.N. Laveaga ¹⁰⁹, R. Lavicka ¹⁰², R. Lea ^{134,55}, H. Lee ¹⁰⁴, I. Legrand ⁴⁵, G. Legras ¹²⁶, J. Lehrbach ³⁸, A.M. Lejeune ³⁴, T.M. Lelek ², R.C. Lemmon ^{1,85}, I. León Monzón ¹⁰⁹, M.M. Lesch ⁹⁵, E.D. Lesser ¹⁸, P. Lévai ⁴⁶, M. Li ⁶, P. Li ¹⁰, X. Li ¹⁰, B.E. Liang-gilman ¹⁸, J. Lien ¹²¹, R. Lietava ¹⁰⁰, I. Likmeta ¹¹⁶, B. Lim ²⁴, S.H. Lim ¹⁶, V. Lindenstruth ³⁸, A. Lindner ⁴⁵, C. Lippmann ⁹⁷, D.H. Liu ⁶, J. Liu ¹¹⁹, G.S.S. Liveraro ¹¹¹, I.M. Lofnes ²⁰, C. Loizides ⁸⁷, S. Lokos ¹⁰⁷, J. Lömker ⁵⁹, X. Lopez ¹²⁷, E. López Torres ⁷, C. Lotteau ¹²⁸, P. Lu ^{97,120}, Z. Lu ¹⁰, F.V. Lugo ⁶⁷, J.R. Luhder ¹²⁶, M. Lunardon ²⁷, G. Luparello ⁵⁷, Y.G. Ma ³⁹, M. Mager ³², A. Maire ¹²⁹, E.M. Majerz ², M.V. Makariev ³⁵, M. Malaev ¹⁴¹, G. Malfattore ²⁵, N.M. Malik ⁹¹, Q.W. Malik ¹⁹, S.K. Malik ⁹¹, L. Malinina ^{I,VIII,142}, D. Mallick ¹³¹, N. Mallick ⁴⁸, G. Mandaglio ^{30,53}, S.K. Mandal ⁷⁹, A. Manea ⁶³, V. Manko ¹⁴¹, F. Manso ¹²⁷, V. Manzari ⁵⁰, Y. Mao ⁶, R.W. Marcjan ², G.V. Margagliotti ²³, A. Margotti ⁵¹, A. Marín ⁹⁷, C. Markert ¹⁰⁸, P. Martinengo ³², M.I. Martínez ⁴⁴, G. Martínez García ¹⁰³, M.P.P. Martins ¹¹⁰, S. Masciocchi ⁹⁷, M. Masera ²⁴, A. Masoni ⁵², L. Massacrier ¹³¹, O. Massen ⁵⁹, A. Mastroserio ^{132,50}, O. Matonoha ⁷⁵, S. Mattiazzzo ²⁷, A. Matyja ¹⁰⁷, A.L. Mazuecos ³², F. Mazzaschi ^{32,24}, M. Mazzilli ¹¹⁶, Y. Melikyan ⁴³, M. Melo ¹¹⁰, A. Menchaca-Rocha ⁶⁷, J.E.M. Mendez ⁶⁵, E. Meninno ¹⁰², A.S. Menon ¹¹⁶, M.W. Menzel ^{32,94}, M. Meres ¹³, Y. Miake ¹²⁵, L. Micheletti ³², D.L. Mihaylov ⁹⁵, K. Mikhaylov ^{142,141}, N. Minafra ¹¹⁸, D. Miśkowiec ⁹⁷, A. Modak ^{134,4}, B. Mohanty ⁸⁰, M. Mohisin Khan ^{V,15}, M.A. Molander ⁴³, S. Monira ¹³⁶, C. Mordasini ¹¹⁷, D.A. Moreira De Godoy ¹²⁶, I. Morozov ¹⁴¹, A. Morsch ³², T. Mrnjavac ³², V. Muccifora ⁴⁹, S. Muhuri ¹³⁵, J.D. Mulligan ⁷⁴, A. Mulliri ²², M.G. Munhoz ¹¹⁰, R.H. Munzer ⁶⁴, H. Murakami ¹²⁴, S. Murray ¹¹⁴, L. Musa ³², J. Musinsky ⁶⁰, J.W. Myrcha ¹³⁶, B. Naik ¹²³, A.I. Nambrath ¹⁸, B.K. Nandi ⁴⁷, R. Nania ⁵¹, E. Nappi ⁵⁰, A.F. Nassirpour ¹⁷, A. Nath ⁹⁴, S. Nath ¹³⁵, C. Natrass ¹²², M.N. Naydenov ³⁵, A. Neagu ¹⁹, A. Negru ¹¹³, E. Nekrasova ¹⁴¹, L. Nellen ⁶⁵, R. Nepeivoda ⁷⁵, S. Nese ¹⁹, N. Nicassio ⁵⁰, B.S. Nielsen ⁸³, E.G. Nielsen ⁸³, S. Nikolaev ¹⁴¹, S. Nikulin ¹⁴¹, V. Nikulin ¹⁴¹, F. Noferini ⁵¹, S. Noh ¹², P. Nomokonov ¹⁴²,

- J. Norman ¹¹⁹, N. Novitzky ⁸⁷, P. Nowakowski ¹³⁶, A. Nyanin ¹⁴¹, J. Nystrand ²⁰, S. Oh ¹⁷,
 A. Ohlson ⁷⁵, V.A. Okorokov ¹⁴¹, J. Oleniacz ¹³⁶, A. Onnerstad ¹¹⁷, C. Oppedisano ⁵⁶, A. Ortiz
 Velasquez ⁶⁵, J. Otwinowski ¹⁰⁷, M. Oya ⁹², K. Oyama ⁷⁶, Y. Pachmayer ⁹⁴, S. Padhan ⁴⁷,
 D. Pagano ^{134,55}, G. Paić ⁶⁵, S. Paisano-Guzmán ⁴⁴, A. Palasciano ⁵⁰, S. Panebianco ¹³⁰,
 C. Pantouvakis ²⁷, H. Park ¹²⁵, H. Park ¹⁰⁴, J. Park ¹²⁵, J.E. Parkkila ³², Y. Patley ⁴⁷, R.N. Patra ⁵⁰,
 B. Paul ¹³⁵, H. Pei ⁶, T. Peitzmann ⁵⁹, X. Peng ¹¹, M. Pennisi ²⁴, S. Perciballi ²⁴, D. Peresunko ¹⁴¹,
 G.M. Perez ⁷, Y. Pestov ¹⁴¹, M.T. Petersen ⁸³, V. Petrov ¹⁴¹, M. Petrovici ⁴⁵, S. Piano ⁵⁷, M. Pikna ¹³,
 P. Pillot ¹⁰³, O. Pinazza ^{51,32}, L. Pinsky ¹¹⁶, C. Pinto ⁹⁵, S. Pisano ⁴⁹, M. Płoskoń ⁷⁴, M. Planinic ⁸⁹,
 F. Pliquet ⁶⁴, D.K. Plociennik ², M.G. Poghosyan ⁸⁷, B. Polichtchouk ¹⁴¹, S. Politano ²⁹, N. Poljak ⁸⁹,
 A. Pop ⁴⁵, S. Porteboeuf-Houssais ¹²⁷, V. Pozdniakov ^{I,142}, I.Y. Pozos ⁴⁴, K.K. Pradhan ⁴⁸,
 S.K. Prasad ⁴, S. Prasad ⁴⁸, R. Preghenella ⁵¹, F. Prino ⁵⁶, C.A. Pruneau ¹³⁷, I. Pshenichnov ¹⁴¹,
 M. Puccio ³², S. Pucillo ²⁴, S. Qiu ⁸⁴, L. Quaglia ²⁴, S. Ragoni ¹⁴, A. Rai ¹³⁸,
 A. Rakotozafindrabe ¹³⁰, L. Ramello ^{133,56}, F. Rami ¹²⁹, M. Rasa ²⁶, S.S. Räsänen ⁴³, R. Rath ⁵¹,
 M.P. Rauch ²⁰, I. Ravasenga ³², K.F. Read ^{87,122}, C. Reckziegel ¹¹², A.R. Redelbach ³⁸,
 K. Redlich ^{VI,79}, C.A. Reetz ⁹⁷, H.D. Regules-Medel ⁴⁴, A. Rehman ²⁰, F. Reidt ³², H.A. Reme-Ness ³⁷,
 Z. Rescakova ³⁶, K. Reygers ⁹⁴, A. Riabov ¹⁴¹, V. Riabov ¹⁴¹, R. Ricci ²⁸, M. Richter ²⁰,
 A.A. Riedel ⁹⁵, W. Riegler ³², A.G. Rifferto ²⁴, M. Rignanese ²⁷, C. Ripoli ²⁸, C. Ristea ⁶³,
 M.V. Rodriguez ³², M. Rodríguez Cahuantzi ⁴⁴, S.A. Rodríguez Ramírez ⁴⁴, K. Røed ¹⁹, R. Rogalev ¹⁴¹,
 E. Rogochaya ¹⁴², T.S. Rogoschinski ⁶⁴, D. Rohr ³², D. Röhrich ²⁰, S. Rojas Torres ³⁴, P.S. Rokita ¹³⁶,
 G. Romanenko ²⁵, F. Ronchetti ³², E.D. Rosas ⁶⁵, K. Roslon ¹³⁶, A. Rossi ⁵⁴, A. Roy ⁴⁸, S. Roy ⁴⁷,
 N. Rubini ^{51,25}, J.A. Rudolph ⁸⁴, D. Ruggiano ¹³⁶, R. Rui ²³, P.G. Russek ², R. Russo ⁸⁴,
 A. Rustamov ⁸¹, E. Ryabinkin ¹⁴¹, Y. Ryabov ¹⁴¹, A. Rybicki ¹⁰⁷, J. Ryu ¹⁶, W. Rzesz ¹³⁶, B. Sabiu ⁵¹,
 S. Sadovsky ¹⁴¹, J. Saetre ²⁰, K. Šafařík ^{I,34}, S. Saha ⁸⁰, B. Sahoo ⁴⁸, R. Sahoo ⁴⁸, S. Sahoo ⁶¹,
 D. Sahu ⁴⁸, P.K. Sahu ⁶¹, J. Saini ¹³⁵, K. Sajdakova ³⁶, S. Sakai ¹²⁵, M.P. Salván ⁹⁷, S. Sambyal ⁹¹,
 D. Samitz ¹⁰², I. Sanna ^{32,95}, T.B. Saramela ¹¹⁰, D. Sarkar ⁸³, P. Sarma ⁴¹, V. Sarritzu ²², V.M. Sarti ⁹⁵,
 M.H.P. Sas ³², S. Sawan ⁸⁰, E. Scapparone ⁵¹, J. Schambach ⁸⁷, H.S. Scheid ⁶⁴, C. Schiaua ⁴⁵,
 R. Schicker ⁹⁴, F. Schlepper ⁹⁴, A. Schmah ⁹⁷, C. Schmidt ⁹⁷, H.R. Schmidt ⁹³, M.O. Schmidt ³²,
 M. Schmidt ⁹³, N.V. Schmidt ⁸⁷, A.R. Schmier ¹²², R. Schotter ^{102,129}, A. Schröter ³⁸, J. Schukraft ³²,
 K. Schweda ⁹⁷, G. Scioli ²⁵, E. Scomparin ⁵⁶, J.E. Seger ¹⁴, Y. Sekiguchi ¹²⁴, D. Sekihata ¹²⁴,
 M. Selina ⁸⁴, I. Selyuzhenkov ⁹⁷, S. Senyukov ¹²⁹, J.J. Seo ⁹⁴, D. Serebryakov ¹⁴¹, L. Serkin ^{VII,65},
 L. Šerkšnytė ⁹⁵, A. Sevcenco ⁶³, T.J. Shaba ⁶⁸, A. Shabetai ¹⁰³, R. Shahoyan ³², A. Shangaraev ¹⁴¹,
 B. Sharma ⁹¹, D. Sharma ⁴⁷, H. Sharma ⁵⁴, M. Sharma ⁹¹, S. Sharma ⁷⁶, S. Sharma ⁹¹, U. Sharma ⁹¹,
 A. Shatat ¹³¹, O. Sheibani ¹¹⁶, K. Shigaki ⁹², M. Shimomura ⁷⁷, J. Shin ¹², S. Shirinkin ¹⁴¹, Q. Shou ³⁹,
 Y. Sibiriak ¹⁴¹, S. Siddhanta ⁵², T. Siemarczuk ⁷⁹, T.F. Silva ¹¹⁰, D. Silvermyr ⁷⁵,
 T. Simantathammakul ¹⁰⁵, R. Simeonov ³⁵, B. Singh ⁹¹, B. Singh ⁹⁵, K. Singh ⁴⁸, R. Singh ⁸⁰,
 R. Singh ⁹¹, R. Singh ⁹⁷, S. Singh ¹⁵, V.K. Singh ¹³⁵, V. Singhal ¹³⁵, T. Sinha ⁹⁹, B. Sitar ¹³,
 M. Sitta ^{133,56}, T.B. Skaali ¹⁹, G. Skorodumovs ⁹⁴, N. Smirnov ¹³⁸, R.J.M. Snellings ⁵⁹, E.H. Solheim ¹⁹,
 J. Song ¹⁶, C. Sonnabend ^{32,97}, J.M. Sonneveld ⁸⁴, F. Soramel ²⁷, A.B. Soto-hernandez ⁸⁸,
 R. Spijkers ⁸⁴, I. Sputowska ¹⁰⁷, J. Staa ⁷⁵, J. Stachel ⁹⁴, I. Stan ⁶³, P.J. Steffanic ¹²², T. Stellhorn ¹²⁶,
 S.F. Stiefelmaier ⁹⁴, D. Stocco ¹⁰³, I. Storehaug ¹⁹, N.J. Strangmann ⁶⁴, P. Stratmann ¹²⁶, S. Strazzi ²⁵,
 A. Sturniolo ^{30,53}, C.P. Stylianidis ⁸⁴, A.A.P. Suade ¹¹⁰, C. Suire ¹³¹, M. Sukhanov ¹⁴¹, M. Suljic ³²,
 R. Sultanov ¹⁴¹, V. Sumberia ⁹¹, S. Sumowidagdo ⁸², M. Szymkowski ¹³⁶, L.H. Tabares ⁷,
 S.F. Taghavi ⁹⁵, G. Taillepied ⁹⁷, J. Takahashi ¹¹¹, G.J. Tambave ⁸⁰, S. Tang ⁶, Z. Tang ¹²⁰, J.D. Tapia
 Takaki ¹¹⁸, N. Tapus ¹¹³, L.A. Tarasovicova ¹²⁶, M.G. Tarzila ⁴⁵, G.F. Tassielli ³¹, A. Tauro ³², A. Tavira
 García ¹³¹, G. Tejeda Muñoz ⁴⁴, L. Terlizzi ²⁴, C. Terrevoli ⁵⁰, S. Thakur ⁴, D. Thomas ¹⁰⁸,
 A. Tikhonov ¹⁴¹, N. Tiltmann ^{32,126}, A.R. Timmins ¹¹⁶, M. Tkacik ¹⁰⁶, T. Tkacik ¹⁰⁶, A. Toia ⁶⁴,
 R. Tokumoto ⁹², S. Tomassini ²⁵, K. Tomohiro ⁹², N. Topilskaya ¹⁴¹, M. Toppi ⁴⁹, V.V. Torres ¹⁰³,
 A.G. Torres Ramos ³¹, A. Trifiró ^{30,53}, T. Triloki ⁹⁶, A.S. Triolo ^{32,30,53}, S. Tripathy ³², T. Tripathy ⁴⁷,
 V. Trubnikov ³, W.H. Trzaska ¹¹⁷, T.P. Trzciński ¹³⁶, C. Tsolanta ¹⁹, R. Tu ³⁹, A. Tumkin ¹⁴¹,
 R. Turrisi ⁵⁴, T.S. Tveter ¹⁹, K. Ullaland ²⁰, B. Ulukutlu ⁹⁵, S. Upadhyaya ¹⁰⁷, A. Uras ¹²⁸,
 M. Urioni ¹³⁴, G.L. Usai ²², M. Vala ³⁶, N. Valle ⁵⁵, L.V.R. van Doremalen ⁵⁹, M. van Leeuwen ⁸⁴,
 C.A. van Veen ⁹⁴, R.J.G. van Weelden ⁸⁴, P. Vande Vyvre ³², D. Varga ⁴⁶, Z. Varga ⁴⁶,
 P. Vargas Torres ⁶⁵, M. Vasileiou ⁷⁸, A. Vasiliev ^{I,141}, O. Vázquez Doce ⁴⁹, O. Vazquez Rueda ¹¹⁶,
 V. Vechernin ¹⁴¹, E. Vercellin ²⁴, S. Vergara Limón ⁴⁴, R. Verma ⁴⁷, L. Vermunt ⁹⁷, R. Vértesi ⁴⁶,
 M. Verweij ⁵⁹, L. Vickovic ³³, Z. Vilakazi ¹²³, O. Villalobos Baillie ¹⁰⁰, A. Villani ²³, A. Vinogradov ¹⁴¹,
 T. Virgili ²⁸, M.M.O. Virta ¹¹⁷, A. Vodopyanov ¹⁴², B. Volkel ³², M.A. Völkl ⁹⁴, S.A. Voloshin ¹³⁷,

G. Volpe ³¹, B. von Haller ³², I. Vorobyev ³², N. Vozniuk ¹⁴¹, J. Vrláková ³⁶, J. Wan³⁹, C. Wang ³⁹, D. Wang³⁹, Y. Wang ³⁹, Y. Wang ⁶, Z. Wang ³⁹, A. Wegrzynek ³², F.T. Weiglhofer³⁸, S.C. Wenzel ³², J.P. Wessels ¹²⁶, J. Wiechula ⁶⁴, J. Wikne ¹⁹, G. Wilk ⁷⁹, J. Wilkinson ⁹⁷, G.A. Willems ¹²⁶, B. Windelband ⁹⁴, M. Winn ¹³⁰, J.R. Wright ¹⁰⁸, W. Wu³⁹, Y. Wu ¹²⁰, Z. Xiong ¹²⁰, R. Xu ⁶, A. Yadav ⁴², A.K. Yadav ¹³⁵, Y. Yamaguchi ⁹², S. Yang²⁰, S. Yano ⁹², E.R. Yeats¹⁸, Z. Yin ⁶, I.-K. Yoo ¹⁶, J.H. Yoon ⁵⁸, H. Yu¹², S. Yuan²⁰, A. Yuncu ⁹⁴, V. Zaccolo ²³, C. Zampolli ³², F. Zanone ⁹⁴, N. Zardoshti ³², A. Zarochentsev ¹⁴¹, P. Závada ⁶², N. Zaviyalov¹⁴¹, M. Zhalov ¹⁴¹, B. Zhang ^{94,6}, C. Zhang ¹³⁰, L. Zhang ³⁹, M. Zhang ^{127,6}, M. Zhang ⁶, S. Zhang ³⁹, X. Zhang ⁶, Y. Zhang¹²⁰, Z. Zhang ⁶, M. Zhao ¹⁰, V. Zhrebchevskii ¹⁴¹, Y. Zhi¹⁰, D. Zhou ⁶, Y. Zhou ⁸³, J. Zhu ^{54,6}, S. Zhu¹²⁰, Y. Zhu⁶, S.C. Zugravel ⁵⁶, N. Zurlo ^{134,55}

Affiliation Notes

^I Deceased

^{II} Also at: Max-Planck-Institut fur Physik, Munich, Germany

^{III} Also at: Italian National Agency for New Technologies, Energy and Sustainable Economic Development (ENEA), Bologna, Italy

^{IV} Also at: Dipartimento DET del Politecnico di Torino, Turin, Italy

^V Also at: Department of Applied Physics, Aligarh Muslim University, Aligarh, India

^{VI} Also at: Institute of Theoretical Physics, University of Wroclaw, Poland

^{VII} Also at: Facultad de Ciencias, Universidad Nacional Autónoma de México, Mexico City, Mexico

^{VIII} Also at: An institution covered by a cooperation agreement with CERN

Collaboration Institutes

¹ A.I. Alikhanyan National Science Laboratory (Yerevan Physics Institute) Foundation, Yerevan, Armenia

² AGH University of Krakow, Cracow, Poland

³ Bogolyubov Institute for Theoretical Physics, National Academy of Sciences of Ukraine, Kiev, Ukraine

⁴ Bose Institute, Department of Physics and Centre for Astroparticle Physics and Space Science (CAPSS), Kolkata, India

⁵ California Polytechnic State University, San Luis Obispo, California, United States

⁶ Central China Normal University, Wuhan, China

⁷ Centro de Aplicaciones Tecnológicas y Desarrollo Nuclear (CEADEN), Havana, Cuba

⁸ Centro de Investigación y de Estudios Avanzados (CINVESTAV), Mexico City and Mérida, Mexico

⁹ Chicago State University, Chicago, Illinois, United States

¹⁰ China Institute of Atomic Energy, Beijing, China

¹¹ China University of Geosciences, Wuhan, China

¹² Chungbuk National University, Cheongju, Republic of Korea

¹³ Comenius University Bratislava, Faculty of Mathematics, Physics and Informatics, Bratislava, Slovak Republic

¹⁴ Creighton University, Omaha, Nebraska, United States

¹⁵ Department of Physics, Aligarh Muslim University, Aligarh, India

¹⁶ Department of Physics, Pusan National University, Pusan, Republic of Korea

¹⁷ Department of Physics, Sejong University, Seoul, Republic of Korea

¹⁸ Department of Physics, University of California, Berkeley, California, United States

¹⁹ Department of Physics, University of Oslo, Oslo, Norway

²⁰ Department of Physics and Technology, University of Bergen, Bergen, Norway

²¹ Dipartimento di Fisica, Università di Pavia, Pavia, Italy

²² Dipartimento di Fisica dell'Università and Sezione INFN, Cagliari, Italy

²³ Dipartimento di Fisica dell'Università and Sezione INFN, Trieste, Italy

²⁴ Dipartimento di Fisica dell'Università and Sezione INFN, Turin, Italy

²⁵ Dipartimento di Fisica e Astronomia dell'Università and Sezione INFN, Bologna, Italy

²⁶ Dipartimento di Fisica e Astronomia dell'Università and Sezione INFN, Catania, Italy

²⁷ Dipartimento di Fisica e Astronomia dell'Università and Sezione INFN, Padova, Italy

²⁸ Dipartimento di Fisica 'E.R. Caianiello' dell'Università and Gruppo Collegato INFN, Salerno, Italy

²⁹ Dipartimento DISAT del Politecnico and Sezione INFN, Turin, Italy

³⁰ Dipartimento di Scienze MIFT, Università di Messina, Messina, Italy

- ³¹ Dipartimento Interateneo di Fisica ‘M. Merlin’ and Sezione INFN, Bari, Italy
³² European Organization for Nuclear Research (CERN), Geneva, Switzerland
³³ Faculty of Electrical Engineering, Mechanical Engineering and Naval Architecture, University of Split, Split, Croatia
³⁴ Faculty of Nuclear Sciences and Physical Engineering, Czech Technical University in Prague, Prague, Czech Republic
³⁵ Faculty of Physics, Sofia University, Sofia, Bulgaria
³⁶ Faculty of Science, P.J. Šafárik University, Košice, Slovak Republic
³⁷ Faculty of Technology, Environmental and Social Sciences, Bergen, Norway
³⁸ Frankfurt Institute for Advanced Studies, Johann Wolfgang Goethe-Universität Frankfurt, Frankfurt, Germany
³⁹ Fudan University, Shanghai, China
⁴⁰ Gangneung-Wonju National University, Gangneung, Republic of Korea
⁴¹ Gauhati University, Department of Physics, Guwahati, India
⁴² Helmholtz-Institut für Strahlen- und Kernphysik, Rheinische Friedrich-Wilhelms-Universität Bonn, Bonn, Germany
⁴³ Helsinki Institute of Physics (HIP), Helsinki, Finland
⁴⁴ High Energy Physics Group, Universidad Autónoma de Puebla, Puebla, Mexico
⁴⁵ Horia Hulubei National Institute of Physics and Nuclear Engineering, Bucharest, Romania
⁴⁶ HUN-REN Wigner Research Centre for Physics, Budapest, Hungary
⁴⁷ Indian Institute of Technology Bombay (IIT), Mumbai, India
⁴⁸ Indian Institute of Technology Indore, Indore, India
⁴⁹ INFN, Laboratori Nazionali di Frascati, Frascati, Italy
⁵⁰ INFN, Sezione di Bari, Bari, Italy
⁵¹ INFN, Sezione di Bologna, Bologna, Italy
⁵² INFN, Sezione di Cagliari, Cagliari, Italy
⁵³ INFN, Sezione di Catania, Catania, Italy
⁵⁴ INFN, Sezione di Padova, Padova, Italy
⁵⁵ INFN, Sezione di Pavia, Pavia, Italy
⁵⁶ INFN, Sezione di Torino, Turin, Italy
⁵⁷ INFN, Sezione di Trieste, Trieste, Italy
⁵⁸ Inha University, Incheon, Republic of Korea
⁵⁹ Institute for Gravitational and Subatomic Physics (GRASP), Utrecht University/Nikhef, Utrecht, Netherlands
⁶⁰ Institute of Experimental Physics, Slovak Academy of Sciences, Košice, Slovak Republic
⁶¹ Institute of Physics, Homi Bhabha National Institute, Bhubaneswar, India
⁶² Institute of Physics of the Czech Academy of Sciences, Prague, Czech Republic
⁶³ Institute of Space Science (ISS), Bucharest, Romania
⁶⁴ Institut für Kernphysik, Johann Wolfgang Goethe-Universität Frankfurt, Frankfurt, Germany
⁶⁵ Instituto de Ciencias Nucleares, Universidad Nacional Autónoma de México, Mexico City, Mexico
⁶⁶ Instituto de Física, Universidade Federal do Rio Grande do Sul (UFRGS), Porto Alegre, Brazil
⁶⁷ Instituto de Física, Universidad Nacional Autónoma de México, Mexico City, Mexico
⁶⁸ iThemba LABS, National Research Foundation, Somerset West, South Africa
⁶⁹ Jeonbuk National University, Jeonju, Republic of Korea
⁷⁰ Johann-Wolfgang-Goethe Universität Frankfurt Institut für Informatik, Fachbereich Informatik und Mathematik, Frankfurt, Germany
⁷¹ Korea Institute of Science and Technology Information, Daejeon, Republic of Korea
⁷² KTO Karatay University, Konya, Turkey
⁷³ Laboratoire de Physique Subatomique et de Cosmologie, Université Grenoble-Alpes, CNRS-IN2P3, Grenoble, France
⁷⁴ Lawrence Berkeley National Laboratory, Berkeley, California, United States
⁷⁵ Lund University Department of Physics, Division of Particle Physics, Lund, Sweden
⁷⁶ Nagasaki Institute of Applied Science, Nagasaki, Japan
⁷⁷ Nara Women’s University (NWU), Nara, Japan
⁷⁸ National and Kapodistrian University of Athens, School of Science, Department of Physics , Athens, Greece
⁷⁹ National Centre for Nuclear Research, Warsaw, Poland
⁸⁰ National Institute of Science Education and Research, Homi Bhabha National Institute, Jatni, India
⁸¹ National Nuclear Research Center, Baku, Azerbaijan

- ⁸² National Research and Innovation Agency - BRIN, Jakarta, Indonesia
⁸³ Niels Bohr Institute, University of Copenhagen, Copenhagen, Denmark
⁸⁴ Nikhef, National institute for subatomic physics, Amsterdam, Netherlands
⁸⁵ Nuclear Physics Group, STFC Daresbury Laboratory, Daresbury, United Kingdom
⁸⁶ Nuclear Physics Institute of the Czech Academy of Sciences, Husinec-Řež, Czech Republic
⁸⁷ Oak Ridge National Laboratory, Oak Ridge, Tennessee, United States
⁸⁸ Ohio State University, Columbus, Ohio, United States
⁸⁹ Physics department, Faculty of science, University of Zagreb, Zagreb, Croatia
⁹⁰ Physics Department, Panjab University, Chandigarh, India
⁹¹ Physics Department, University of Jammu, Jammu, India
⁹² Physics Program and International Institute for Sustainability with Knotted Chiral Meta Matter (WPI-SKCM²), Hiroshima University, Hiroshima, Japan
⁹³ Physikalisches Institut, Eberhard-Karls-Universität Tübingen, Tübingen, Germany
⁹⁴ Physikalisches Institut, Ruprecht-Karls-Universität Heidelberg, Heidelberg, Germany
⁹⁵ Physik Department, Technische Universität München, Munich, Germany
⁹⁶ Politecnico di Bari and Sezione INFN, Bari, Italy
⁹⁷ Research Division and ExtreMe Matter Institute EMMI, GSI Helmholtzzentrum für Schwerionenforschung GmbH, Darmstadt, Germany
⁹⁸ Saga University, Saga, Japan
⁹⁹ Saha Institute of Nuclear Physics, Homi Bhabha National Institute, Kolkata, India
¹⁰⁰ School of Physics and Astronomy, University of Birmingham, Birmingham, United Kingdom
¹⁰¹ Sección Física, Departamento de Ciencias, Pontificia Universidad Católica del Perú, Lima, Peru
¹⁰² Stefan Meyer Institut für Subatomare Physik (SMI), Vienna, Austria
¹⁰³ SUBATECH, IMT Atlantique, Nantes Université, CNRS-IN2P3, Nantes, France
¹⁰⁴ Sungkyunkwan University, Suwon City, Republic of Korea
¹⁰⁵ Suranaree University of Technology, Nakhon Ratchasima, Thailand
¹⁰⁶ Technical University of Košice, Košice, Slovak Republic
¹⁰⁷ The Henryk Niewodniczanski Institute of Nuclear Physics, Polish Academy of Sciences, Cracow, Poland
¹⁰⁸ The University of Texas at Austin, Austin, Texas, United States
¹⁰⁹ Universidad Autónoma de Sinaloa, Culiacán, Mexico
¹¹⁰ Universidade de São Paulo (USP), São Paulo, Brazil
¹¹¹ Universidade Estadual de Campinas (UNICAMP), Campinas, Brazil
¹¹² Universidade Federal do ABC, Santo Andre, Brazil
¹¹³ Universitatea Nationala de Stiinta si Tehnologie Politehnica Bucuresti, Bucharest, Romania
¹¹⁴ University of Cape Town, Cape Town, South Africa
¹¹⁵ University of Derby, Derby, United Kingdom
¹¹⁶ University of Houston, Houston, Texas, United States
¹¹⁷ University of Jyväskylä, Jyväskylä, Finland
¹¹⁸ University of Kansas, Lawrence, Kansas, United States
¹¹⁹ University of Liverpool, Liverpool, United Kingdom
¹²⁰ University of Science and Technology of China, Hefei, China
¹²¹ University of South-Eastern Norway, Kongsberg, Norway
¹²² University of Tennessee, Knoxville, Tennessee, United States
¹²³ University of the Witwatersrand, Johannesburg, South Africa
¹²⁴ University of Tokyo, Tokyo, Japan
¹²⁵ University of Tsukuba, Tsukuba, Japan
¹²⁶ Universität Münster, Institut für Kernphysik, Münster, Germany
¹²⁷ Université Clermont Auvergne, CNRS/IN2P3, LPC, Clermont-Ferrand, France
¹²⁸ Université de Lyon, CNRS/IN2P3, Institut de Physique des 2 Infinis de Lyon, Lyon, France
¹²⁹ Université de Strasbourg, CNRS, IPHC UMR 7178, F-67000 Strasbourg, France, Strasbourg, France
¹³⁰ Université Paris-Saclay, Centre d'Etudes de Saclay (CEA), IRFU, Département de Physique Nucléaire (DPhN), Saclay, France
¹³¹ Université Paris-Saclay, CNRS/IN2P3, IJCLab, Orsay, France
¹³² Università degli Studi di Foggia, Foggia, Italy
¹³³ Università del Piemonte Orientale, Vercelli, Italy
¹³⁴ Università di Brescia, Brescia, Italy

¹³⁵ Variable Energy Cyclotron Centre, Homi Bhabha National Institute, Kolkata, India

¹³⁶ Warsaw University of Technology, Warsaw, Poland

¹³⁷ Wayne State University, Detroit, Michigan, United States

¹³⁸ Yale University, New Haven, Connecticut, United States

¹³⁹ Yonsei University, Seoul, Republic of Korea

¹⁴⁰ Zentrum für Technologie und Transfer (ZTT), Worms, Germany

¹⁴¹ Affiliated with an institute covered by a cooperation agreement with CERN

¹⁴² Affiliated with an international laboratory covered by a cooperation agreement with CERN.